Addis Ababa University

Addis Ababa Institute of Technology

School of Electrical and Computer Engineering

Sensorless Control of Surface Mounted Permanent Magnet Synchronous Motor using Fractional Order Sliding Mode Control

A thesis submitted to School of Graduate Studies, Addis Ababa Institute of Technology, Addis Ababa University in partial fulfillment of the requirement for the Degree of Master of Science in Electrical Engineering (Control Engineering)

By

Ayantu Getachew

Advisor

Mengesha Mamo (PhD)

January 30, 2025

Addis Ababa, Ethiopia

Addis Ababa University

Addis Ababa Institute of Technology

School of Electrical and Computer Engineering

Sensorless Control of Surface Mounted Permanent Magnet Synchronous Motor using Fractional Order Sliding Mode Control

By

Ayantu Getachew

Approved by Examining Board of:

Dean, School of Graduate Committee	Signature	Date
_____	_____	_____
Advisor	Signature	Date
_____	_____	_____
Internal Examiner	Signature	Date
_____	_____	_____
External Examiner	Signature	Date
_____	_____	_____

Declaration

I, the undersigned, declare that this MSc thesis is my original work, has not been presented for fulfillment of any degree in this or any other university and all sources and materials used for the thesis are acknowledged.

Author

Ayantu Getachew

Signature

_____

Place:

Addis Ababa Institute of Technology, AAiT
Addis Ababa University, AAU
Addis Ababa, Ethiopia.
Submitted by: January 30, 2025.

This thesis has been submitted for examination with my approval under university advisor Mengesha Mamo (PhD).

Dedication

To my beloved family,

This thesis is dedicated to you. Your unwavering support, patience, and encouragement have been the foundation upon which I have built my academic journey. Your belief in me has been a constant source of strength and inspiration, making this achievement possible.

To my parents, whose sacrifices and guidance have shaped who I am today; to my siblings, who have always been there with a listening ear and a word of encouragement; and to my entire family, whose love and support have been my greatest motivation.

Thank you for being my rock and my greatest cheerleaders.

With all my love and gratitude,

Ayantu Getachew

Acknowledgment

First and foremost, praises and thanks to the God, the Almighty, for His showers of blessings throughout my thesis work to complete successfully. I would like to express my deep and sincere gratitude to my Advisor, Dr. Mengesha Mamo, Associate Professor, School of Electrical and Computer Engineering, Addis Ababa Institute of Technology (AAiT), Addis Ababa University (AAU). for giving me the opportunity to do thesis and providing invaluable guidance throughout this thesis. He has taught me the methodology to carry out the thesis and to present the thesis works as clearly as possible. It was a great privilege and honor to work and study under his guidance. I am extremely grateful for what he has offered me. I am extremely grateful to my parents for their love, understanding, prayers and continuing support to complete this research work.

Finally, my thanks go to all the people who have supported me to complete the thesis work directly or indirectly.

Abstract

This research presents Sliding Mode Speed Estimator (SMSE) and Fractional Order Sliding Mode Control (FOSMC) for permanent magnet synchronous motors (PMSM) to achieve high performance sensorless control. The SMSE is able to estimate the rotor position and speed. The back electromotive force SMSE is proposed. The estimated rotor position and speed are used to replace the actual values detected by the sensor. The estimation and PMSM modeling suffer with uncertainty and chattering hence, need robust control method to work efficiently in the whole working ranges of speed. Sensorless speed control suffers with accuracy specifically in the low speed region of the PMSM control due-to estimation and modeling defects. Therefore, FOSMC comes into application for enhancing the performance of PMSM during the transient conditions. Hence, the estimation accuracy is tracked within very short settling time of less than 1 second and the robustness against uncertainties is enhanced. This is verified with simulation results performed using MATLAB Simulink.

Keywords: SPMSM, FOSMC, SMSE, MATLAB, Simulink

Contents

List of Figures

List of Tables

List of Acronyms

ASTNLFOPIDSMC Adaptive super-twisting nonlinear Fractional-order PID sliding mode control

ASTRL Adaptive super-twisting reaching law

CNC Computer numerical control

DC Direct current

EKF Extended Kalman Filter

FOSMC Fractional Order Sliding Mode Control

FOSMC-PID Fractional order sliding mode control with PID

GPC Generalized predictive controller

HFI High-frequency injection

HGO high gain observers

HOTSMO High-order terminal sliding-mode observer

IPMSMs Interior permanent magnet synchronous motor

IPDMs Initial position detection methods

LQG linear quadratic Gaussian

LQR linear quadratic regulators

MATLAB Mathematics Labratory

MMF magneto-motive force

MRAS Model reference adaptive system

NLFOPID Nonlinear fractional order PID

NMPC nonlinear model predictive controller

PID proportional-integral-derivativer

PMSM permanent magnet synchronous motors

SMC sliding mode control

SMO sliding mode observer

SMSE Sliding Mode Speed Estimator

SPMSM surface mounted permanent magnet synchronous motor

STSME super twisting sliding mode speed estimator

STSME Super twisting sliding mode speed estimator

List of Symbols

B - friction damping coefficient

J - moment of inertia

R - resistance

p - Number of pole pairs (a magnet)

P - Power

L - stator inductance

e_a, e_b, e_c - back electromotive force (EMF) in a-b-c stator axis respectively

λ_m - rotor flux linkage

λ_a, λ_b, λ_c - stator flux linkage

θ - electrical angle between rotor axis and stator axis

θ_r - mechanical angular position

ω_r - rotor mechanical speed

ω - synchronous speed

v_a, v_b, v_c - stator voltages in a-b-c axis respectively

i_a, i_b, i_c - stator currents in a-b-c axis respectively

T_e - electromagnetic torque

T_m - electro-mechanical torque

T_L - load torque

Chapter 1

Introduction

1.1 General Background

Permanent magnet synchronous motor (PMSM) is becoming one of the most competitive motion control product because of the inherent advantages of low rotor inertia, high efficiency, and high power density, which has been utilized in industrial applications [1, 2]. Traditionally, achieving accurate speed control in PMSM motors has relied on the use of mechanical position or speed sensors to provide feedback to the control system. However, sensor-based control approaches can introduce complexity, cost, and potential points of failure into the system [1, 2]. In response to these challenges, sensorless control techniques have emerged as a promising solution, aiming to eliminate the need for dedicated sensors and thereby enhancing system robustness and reducing implementation costs.

Model reference adaptive system (MRAS), extended Kalman filter (EKF), high gain observers (HGO), and sliding mode observer (SMO) have been proposed as reliable tools for sensorless estimation of motor speed and rotor position [1, 2, 3, 4]. Relaying on these literatures super twisting sliding mode speed estimator (STSME) is designed in this thesis for speed control of a sensorless PMSM control.

Control of PMSM have been the focus of many researchers. Different control concepts starting from the linear and conventional proportional Integral Derivative (PID) [5], linear quadratic regulators (LQR) [6, 7], linear quadratic Gaussian (LQG) [8, 9], to nonlinear H-2 and H-infinity control [10] methods have been under study. However, the PMSM is

a typical high nonlinear, multivariable coupled system, and its performance is sensitive to external load disturbances, parameter changes in plant, and unmodeled and nonlinear dynamics [11]. Hence, the conventional linear control models are not robust to these systems. Therefore, to achieve good dynamic response, some robust control strategies such as nonlinear control methods of adaptive [12], nonlinear model predictive (NMPC) [13] and sliding mode control (SMC) [1, 2, 4, 11, 13, 14] have been developed.

The SMC is a powerful nonlinear control technique and has been widely used for speed and position control of PMSM system, because it provides a fast dynamic response and is insensitive to external load disturbances and parameter variations [1]. Unlike traditional control methods, SMC actively exploits the dynamics of the system, allowing PMSMs to achieve stable and precise performance even in the presence of parameter variations or external disturbances. This robustness ensures reliable operation across a wide range of operating conditions in PMSM control. Moreover, SMC facilitates fast dynamic response and high precision tracking of desired trajectories, enabling PMSMs to quickly reach and maintain desired operating points with minimal error. This agility and precision enhance the overall performance and efficiency of PMSM-based systems, making them ideal for demanding applications requiring precise control over motor operation.

However, SMC suffer from the drawback of chattering phenomenon, which can introduce undesirable high-frequency oscillations in PMSM systems. The presence of chattering introduce noise and vibration in PMSM systems, leading to increased wear on mechanical components and reduced overall system performance. Therefore, by careful consideration the Fractional Order Sliding Mode Control (FOSMC) is preferred to solve these problems of traditional SMC. The FOSMC is robust in the case of sensorless PMSM control that handles system complexity which results from inherent system nonlinearity, coupling between state variables of speed and current, and actuator saturation [1, 3, 11, 15]. Hence, it solves the shortcomings of traditional SMC; and chattering. Combining FOSMC with STSME presents a compelling approach to achieving sensorless speed control in PMSM, promising improved reliability, accuracy, and cost-effectiveness compared to traditional sensor-based approaches.

1.2 Statement of Problem

Permanent Magnet Synchronous Motors (PMSMs) are extensively utilized in various industrial applications due to their high efficiency and dynamic response. However, accurate speed control of PMSM motors often necessitates the use of position or speed sensors, which escalates system complexity and cost while introducing potential points of failure. Sensorless control technique offers a compelling alternative by eliminating the need for dedicated mechanical sensor, thereby mitigating system complexity, cost, and enhancing reliability. Despite these advantages, challenges persist in implementing sensorless control strategy, including nonlinear motor dynamics, parameter variations, and the necessity for high speed and accurate estimation methods.

To address these challenges, this thesis aims to investigate the design of sensorless speed control strategy for PMSM using fractional order sliding mode control (FOSMC) in combination with super twisting sliding mode estimators (STSME). The thesis focus on theoretical analysis, modeling, and design of these advanced control techniques. The thesis explore the design and simulation of FOSMC and STSME based sensorless speed control systems to evaluate under various operating conditions. Hence, by leveraging the capabilities of FOSMC and STSME, the research seeks to develop more efficient, reliable, and cost-effective motor control system.

1.3 Objective of the Thesis

1.3.1 General Objective

The general objective of the research is to develop and evaluate a fractional order sliding mode control for speed enhancing the performance, stability, and robustness of a sensorless speed control of PMSM.

1.3.2 Specific Objectives

The specific objective of the research are:

- To design super twisting sliding mode speed and position estimator for a sensorless PMSM control.
- To design fractional order sliding mode speed control (FOSMC) and proportional-integral (PI) current controllers for a sensorless PMSM.
- To analyze the performance of designed controllers in the presence of load torque, parameter variation, and transient conditions through MATLAB simulations.

1.4 Significance of the Thesis

This research has the following significant contributions:

- The primary benefit of the proposed method is the removal of speed and position sensors from the motor, which reduces cost, complexity, and failure in the system.
- Utilizing FOSMC in sensorless speed control enables the system less sensitive to variations in motor parameters, load disturbances, and other external factors, hence improved robustness.
- FOSMC offers the potential for improved dynamic response and transient performance compared to traditional control techniques. Better speed regulation, faster transient response, and smoother operation of the PMSM motor.
- FOSMC's inherent ability to handle nonlinear systems makes it a suitable candidate for sensorless speed control, as it effectively cope with non-linearities in the motor and drive system under low speed and load conditions.
- Fractional order integration and differentiation can provide better estimation of the motor's speed and rotor position, leading to more precise control and improved overall performance.

1.5 Methodology

The basic procedures to complete the thesis and meet specified objectives of research are shown in the following flowchart, 1.1.

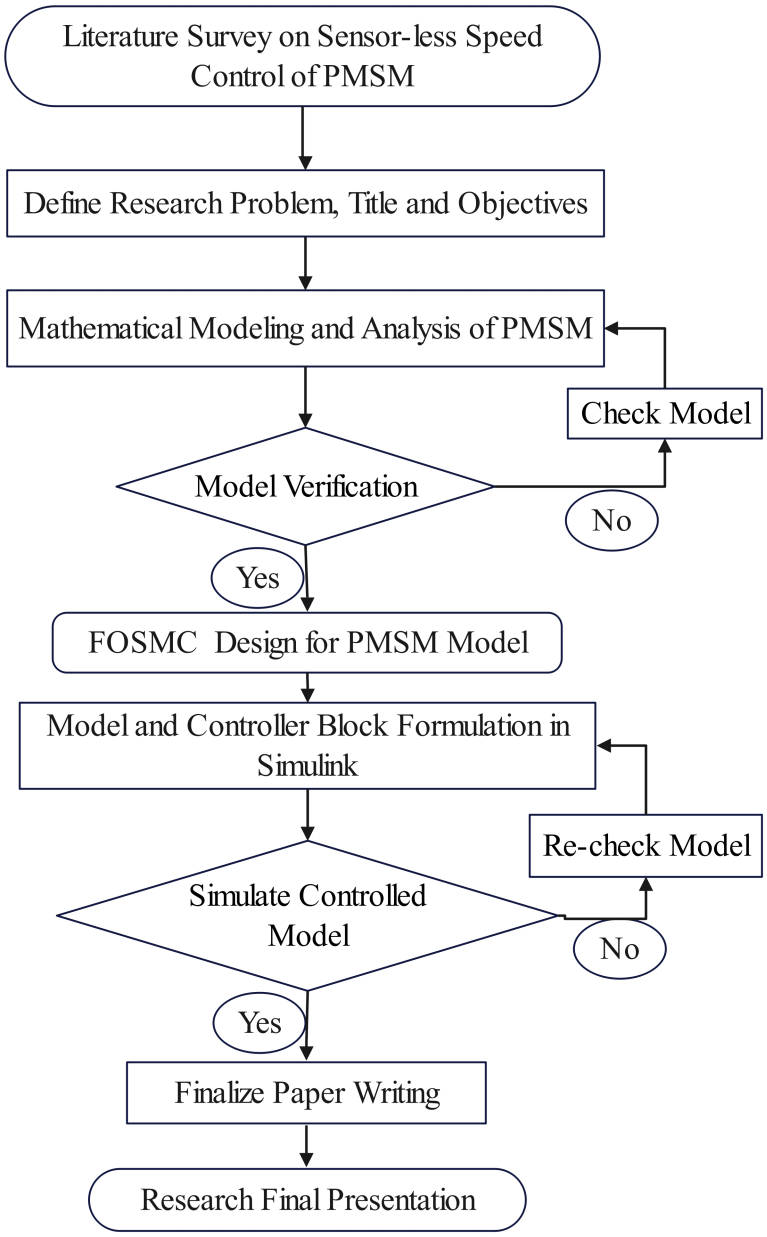

Figure 1.1: Methodology

1.6 Scope and Limitation of Thesis

The scope of the thesis encompasses theoretical analysis, modeling, and simulation studies aimed at developing and evaluating sensorless control strategy for PMSM. The research focus on investigating the dynamic behavior of PMSM motors and the theoretical principles underlying FOSMC and STSME. The scope includes the design and validation of mathematical models for PMSM motors and the integration of FOSMC and STSME algorithms into simulation environments for comprehensive analysis.

The applicability of the proposed sensorless control strategy to real world PMSM systems need further validation through experimental testing. The accuracy of simulation models subjected to simplifications and assumptions, which impact the generalizability of the results. Additionally, the scope of the thesis constrained by computational resources and simulation tools of MATLAB available for conducting extensive analysis.

1.7 Thesis Outline

The thesis outline is organized by six chapters.

Chapter 1 presents the general introduction about PMSM modeling and control.

Chapter 2 discusses review of various research papers which were significant and used as background concepts for this research to-be done.

Chapter 3 presents the dynamic modeling of PMSM. The working principles of the PMSM is discussed thoroughly.

Chapter 4 presents the super twisting sliding mode estimator and overall control scheme design using fractional order sliding mode control principles.

Chapter 5 discusses the simulation results, and analysis is done based on simulations.

Chapter 6 conclusion is drawn from the overall analysis performed and recommendation for future work are presented.

Chapter 2

Literature Review

In the modern days of electromechanical systems and drive, Permanent Magnet Synchronous Motors (PMSMs) have emerged as stalwart device, revered for their high efficiency, high power density, precision, versatility, and simple structure, which is widely used in many highly dynamic and high-precision engineering applications, such as industrial drive, aerospace, and electric vehicle [1].

The fundamental principles underlying the PMSM operation are vital to assess these applications. At its core, a PMSM operates on the principle of electromagnetic induction, harnessing the interaction between the stator and rotor magnetic fields to produce mechanical motion. The fixed magnets in the rotor bestow upon PMSMs a remarkable level of efficiency and power density, making them indispensable in applications ranging from electric vehicles to precision robotics [16].

The advancement and emerging of power-electronics, and control theory become central to the effective utilization of PMSMs in different applications. This concentrates on the currents flowing through the motor windings, optimizing control, speed regulation, and overall system stability. Various control strategies, from classic field-oriented control to advanced model predictive control and robust control, offer about tailoring motor performance to meet the exact demands of diverse applications [17].

Moreover, the quest for enhanced reliability and cost-effectiveness has galvanize the development of sensorless control techniques for PMSMs [12, 18, 19, 20]. By cleverly exploiting the motor's intrinsic electrical and mechanical properties, sensorless algorithms

enable precise control without the need for cumbersome position or speed sensors. This paradigm shift not only simplifies system design and reduces maintenance but also sets the stage for innovation applications in environments where sensors are impractical or cost-prohibitive.

Hence, throughout this literature a comprehensive exploration of PMSMs from their application area, sensorless design, and control is done. The mysteries of control algorithms, and intricacies of sensorless operation is discussed in the following sections.

2.1 Application of PMSM

Applications of PMSMs span a vast spectrum of industries, owing to their exceptional performance characteristics and efficiency. Within the domain of electric propulsion PMSMs emerge as the cornerstone of a transformative shift, reign supreme, powering electric and hybrid vehicles with unparalleled torque density and energy efficiency. Their compact size, high power density, and precise control make them the propulsion system of choice for everything from electric cars and buses to electric bikes and scooters, driving the transition towards sustainable transportation [1, 4, 13].

Industrial automation is another area where PMSMs are highly used as a dominance machines. These motors find widespread use in robotics, Computer numerical control (CNC) machines, and industrial pumps and compressors, where precise motion control and high torque density are paramount. Their ability to rapidly respond to dynamic load changes and maintain precise speed and position control makes them indispensable in manufacturing processes, enhancing productivity, and product quality while reducing energy consumption [21].

Renewable energy sources harness the power of nature to generate electricity, and PMSMs play a pivotal role in this green revolution. Wind turbines and hydroelectric generators utilize PMSMs for power generation, leveraging their efficiency and reliability to convert kinetic energy into electrical power. With advancements in control algorithms and grid integration, PMSMs enable renewable energy systems to operate seamlessly, contributing to a more sustainable and environmentally friendly energy landscape [22].

Moreover, the aerospace and marine industries benefit immensely from the prowess of PMSMs. Electric propulsion systems employing PMSMs offer a compelling alternative to traditional combustion engines, providing quieter operation, reduced emissions, and greater flexibility in design. From electric aircraft propulsion to electric propulsion systems for ships and submarines, PMSMs are propelling these industries towards a future of cleaner, more efficient transportation, heralding a new era of electrified mobility on land, sea, and air [23].

2.2 Sensorless Design of PMSM

The Sensorless Design of Permanent Magnet Synchronous Motors (PMSMs) stands at the forefront of modern engineering, offering a paradigm shift in motor control technology. By eliminating the need for physical sensors to detect rotor position, sensorless designs promise enhanced reliability, reduced complexity, and lower costs in various applications. This innovative approach leverages advanced algorithms and signal processing techniques to accurately estimate the rotor position based on measurable parameters such as motor currents and voltages. Such advancements enhance the overall efficiency and performance of PMSM-driven systems, marking a significant milestone in the evolution of electric motor technology [24].

Wang et al. (2019), have been studying a review about sensorless control techniques for PMSM drives [16]. The four types of sensorless control techniques: initial position detection methods (IPDMs), low-speed control strategies, mid-high-speed control strategies, and full-speed control strategies have been discussed. The fundamental working principles, their advantages and disadvantages, the control precision, and the application range of these strategies on surface and interior permanent magnet synchronous motors (SPMSMs, IPMSMs) have been also discussed in detail.

Zhao et al. (2021), present an improved super-twisting high-order sliding mode observer design method for PMSMs to achieve high-performance sensorless control [1]. The proposed observer was used to estimate the rotor position and speed, and parameter disturbances simultaneously. The back-EMF model based method was also used for the

sensorless observer to constructed improved estimation effect. The estimation accuracy and robustness against uncertainties was also enhanced.This was proved through simulation and experimental results on the dynamic and steady-state working phases.

Ilioudis et al. (2020), present a sensorless control method for PMSM with magnetic saliency estimation method [20]. The method was applied based on a high-frequency injection (HFI) technique applied on the modified PMSM model in the σ-δ reference frame. A major emphasis was placed on the magnetic saliency estimation to indicate a practical approach in tracking PMSM inductance variations. Further, a sliding mode observer (SMO) was designed to estimate the speed and angle of rotor flux based on equivalent control applying a smooth function of the angle error instead of a sign one to reduce the chattering phenomenon.

2.3 Control Problem of PMSM

Control of PMSMs is very difficult due to complexity and nonlinearity of the model. Different control methods have been under research from the conventional to robust for years, and discussed in the following sections.

2.3.1 Conventional Control of PMSM

Conventional control of PMSMs relies on sensor feedback to regulate motor speed, current and torque. Feedback control form allows for precise control of the motor, ensuring stable operation across a wide range of operating conditions. These methods relay on the feedback and state estimations hence the control needs tobe robust against these uncertainties. The conventional control remained a widely-used approach in various industrial applications for PMSM where high precision and reliability are paramount.

Jan et al. (2008), proposed a robust PID control scheme for the PMSM using a genetic searching approach [25]. Based on a simple genetic algorithm, a set of PID parameters obtained such that the robust stability for the closed-loop system is guaranteed. The proposed method was implemented by a DSP-based fully digital controller. The performances of the controller achieved and proved through the experimental results.

2.3.2 Adaptive Control of PMSM

Adaptive controller design methods extract knowledge of the plant parameters online and redesigns the control law in repetitive manner. This method doesn't need a priori information about the bounds on the uncertain and or time-varying parameters.

Abo-Khalil et al. (2021), proposed model reference adaptive system (MRAS) method to estimate the position and speed of a PMSM by considering the error between real and estimated rotor position values [12]. The proposed method has been tested for various speed and load torque conditions experimentally. The results show good performance and accurate speed-tracking capability when it is compared with the sliding mode observer.

Shao et al. (2019), proposed an optimal speed control strategy for a PMSM system using a generalized predictive controller with a high-order terminal sliding-mode observer (HOTSMO) [13]. The undesirable performance in the presence of system disturbances, including internal model uncertainties and external load disturbances, was analyzed. A robust generalized predictive controller (GPC) with a HOTSMO was applied to achieve a fast response and ensure stronger robustness and improved disturbance rejection performance in a simultaneous fashion. The proposed observer estimates the unknown disturbances with chattering elimination. The proposed methodology was verified through simulations and experimentally, and finally a better speed dynamic response and a stronger robustness was achieved.

Gao et al. (2020), proposed adaptive super-twisting nonlinear Fractional-order PID sliding mode control (ASTNLFOPIDSMC) strategy using extended state observer (ESO) for the speed control of PMSM [3]. The ASTNLFOPIDSMC strategy was constructed by the adaptive super-twisting reaching law (ASTRL) and the nonlinear fractional order PID (NLFOPID) sliding surfaces. ESO was designed to achieve dynamic feedback compensation for external disturbance. The Lyapunov stability theorem and Fractional calculus were used to prove the stability of the system.

2.3.3 Robust Control of PMSM

Huang et al. (2012), proposed a robust fractional-order sliding mode controller (FOSMC) for the position control of a PMSM [11]. The sliding surface of the SMC was designed based on the fractional-order calculus of the state variables. The performance and robustness of the proposed method were analyzed and tested for nonlinear load torque disturbances, and simulation results show that the proposed algorithm is more robust and effective than the conventional SMC method.

Zaihidee et al. (2019), proposed a robust speed control of PMSM using SMC [2]. It was investigated that the current status of implementing SMC for PMSMs. SMC enhancement using fractional order sliding surface design was elaborated and verified by simulation results. Remarkable features as well as disadvantages of previous works were summarized and ideas on possible future works were discussed.

Dominguez et al. (2013), proposed sampled–data model for surface mounted permanent magnet synchronous motors (SMPMSM) based on the symplectic Euler method [4]. Based on the obtained model, a digital sliding mode controller was designed for rotor velocity output tracking. A digital observer was designed for rotor position and velocity, and load estimation. A separation principle was introduced in order to verify the proposed controller. Closed-loop simulations were carried out on a sampled continuous-time controller. The performance of the proposed controller was verified experimentally.

M Zaihidee et al. (2019), proposed fractional order sliding mode control (FOSMC) for speed regulation and control of PMSM [26]. By introducing fractional calculus in the sliding mode manifold, FOSMC was proposed for the speed control loop. Stability of the proposed controller was proved through Lyapunov stability theorem. The methodology was proved in simulation and experimentally: show its superiority in terms of faster convergence, better tracking precision and better anti-disturbance rejection properties than SMC. Chattering effect of FOSMC was seen smaller compared to those of conventional SMC. A comprehensive comparison table was also presented.

Gao et al. (2019), proposed a SMC with nonlinear fractional order PID sliding surface based on a novel extended state observer for the speed operation of a SPMSM [27]. A

novel extended state observer was designed based on the nonlinear functions to achieve dynamic feedback compensation for external disturbances. Stability of the system was proved based on the Lyapunov stability theorem. Comparative simulation results were done to show the good stability, dynamic properties, and strong robustness against external disturbances of the methodology.

Zaihidee et al. (2018), proposed a fractional order sliding mode control with PID sliding surface design (FOSMC-PID) [15]. The controller incorporates fractional calculus which has a slower energy transfer compared to integer order calculus in order to suppress the chattering. Stability of the controller was analyzed using Lyapunov stability theorem. Simulation results proved that the proposed FOSMC speed controller performs as a robust and fast anti-disturbance controller to regulate the speed of a PMSM and proven its advantages against SMC controllers.

Analyzing the existing literatures thoroughly, for the sensorless control of a nonlinear PMSM model, SMC is becoming a more robust and advanced control method. However, there are two main problems to overcome when using the SMC method. The first problem is dealing the effects of unknown internal and external disturbances on the system, which can be solved using adaptive and fuzzy control respectively. The second problem is the chattering and it is solved through the fuzzy, higher order SMC, and FOSMC [1, 2, 11, 13, 14, 19, 28]. Therefore, FOSMC is developed for the speed control loop and PI control designed for current control loops of PMSM that handles both disturbance and chattering.

Chapter 3

Sensorless Permanent Magnet Synchronous Motor Mathematical Modeling

3.1 Working Principle

In this chapter the mathematical modeling of the PMSM is developed using different coordinate axis transformations. The PMSM have an electromagnetic stator and a permanent magnet rotor. The magnetic flux of the rotor is caused by permanent magnets, rather than a direct current, which is the case in DC motors. It has a multi-phase stator and the stator electrical frequency is directly proportional to the rotor speed in the steady state, [14]. However, it differs from a traditional synchronous machine in that it has permanent magnets in place of the field winding, hence has no rotor conductors. The use of permanent magnets in the rotor enhances efficiency, eliminates the need for slip rings, and eliminates the electrical rotor dynamics that complicate control.

There are several design methods for building the rotor in a PMSM. The most notable method in design is the number of magnets or pole pairs mounted, [4]. The number of pole pairs will affect the synchronous speed and the amount of torque the motor yields for a certain current. Another design method is either the rotor magnets are mounted on the

iron core also called surface-mounted-PMSM or the magnets are mounted inside the iron core called internal-mounted-PMSM. The type of mounting will affect the inductance created by the rotor. The inductance of stator winding is generally a function of rotor position. When a stator winding is energized, applying a DC voltage for a certain time, a magnetic field with a fixed direction will be established. The current response of the winding is different due to inductance variation.

However, in this thesis surface mounted PMSM is considered. This is the case of most brush-less motors, and there is no saliency which results the stator self-inductance is independent of the rotor position. A typical PMSM cross sectional view is given by Figure 3.1, [17].

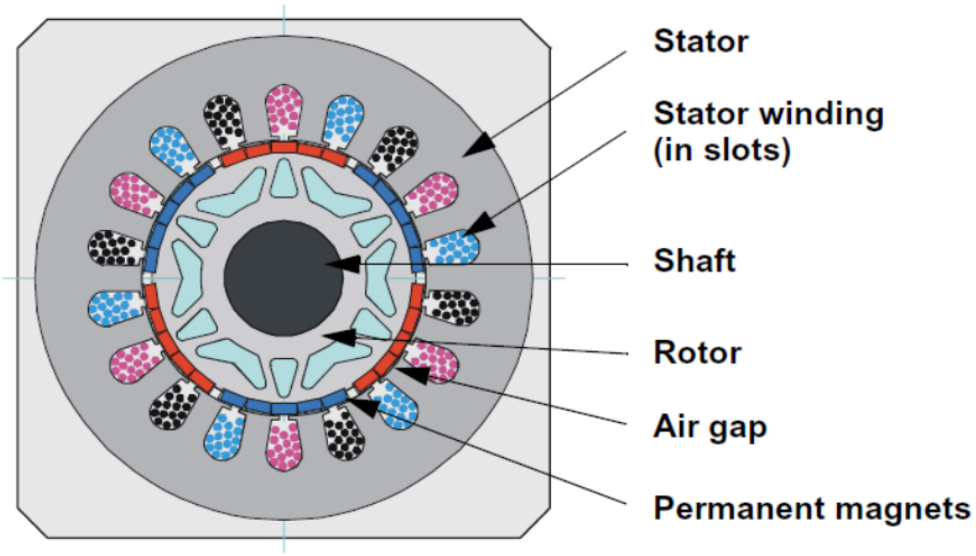

Figure 3.1: Cross Sectional View of PMSM

Every mathematical modeling seeks simplification or engineering assumptions to the real physical system. So in this thesis the following engineering assumptions are considered, [11, 12, 14, 17, 29].

- The saturation and parameter changes are neglected.
- The motor current is symmetrical three phase sine function.
- Stator resistances and inductances of all the windings are equal and symmetrical.

- Eddy currents and hysteresis losses are negligible.
- The induced EMF is sinusoidal.

The following physical variables and constants are used throught the paper, so defining them is vital first.

- R - resistance
- p - Number of pole pairs (a magnet)
- P - Power
- L - stator inductance
- e_a, e_b, e_c - back electromotive force (EMF) in a-b-c stator axis respectively
- λ_m - rotor flux linkage
- λ_a, λ_b, λ_c - stator flux linkage
- θ - electrical angle between rotor axis and stator axis
- θ_r - mechanical angular position of motor
- ω_r - rotor mechanical speed
- ω - synchronous speed
- v_a, v_b, v_c - stator voltages in a-b-c axis respectively
- i_a, i_b, i_c - stator currents in a-b-c axis respectively
- T_e - electromagnetic torque
- T_m - electro-mechanical torque
- T_L - load torque
- J - moment of inertia
- B - friction damping coefficient.

3.1.1 Stator Phase (a-b-c) PMSM Modeling

There are different axis of analysis for complete mathematical modeling of the PMSM. These are a-b-c axis, α-β axis, and d-q axis. In doing these there are two major reference frames (physical frames) of analysis: the fixed stator reference frame and moving rotor reference frame. Let's start from the stator reference frame defining the dynamics of current and voltage equations thoroughly using basic electrical laws.

The SPMSM consists of a stator with a three-phase armature winding and a rotor with a permanent magnet. In the stator, a three-phase winding is electrically wound every 120 degrees, through which the voltage is applied to the motor from the outside, [12]. The armature winding of the stator is composed of coils of several turns, and this winding is induced with a voltage in the stator according to a change in magnetic flux that is linked to the winding. Also, the stator winding has a resistance. Accordingly, the relationship between the stator voltage and the current is as shown by equation 3.1.

$$\begin{aligned} v_a &= Ri_a + \frac{\partial \lambda_a}{\partial t} \\ v_b &= Ri_b + \frac{\partial \lambda_b}{\partial t} \\ v_c &= Ri_c + \frac{\partial \lambda_c}{\partial t} \end{aligned} \tag{3.1}$$

The stator flux linkages are also given as follows.

$$\begin{aligned} \lambda_a &= Li_a + \lambda_m sin(\theta) \\ \lambda_b &= Li_b + \lambda_m sin(\theta - \frac{2\pi}{3}) \\ \lambda_c &= Li_c + \lambda_m sin(\theta + \frac{2\pi}{3}) \end{aligned} \tag{3.2}$$

Now the stator voltage equation 3.1 is simplified and rewritten as follows, equation 3.3.

$$\begin{aligned} v_a &= Ri_a + L\dot{i}_a + \omega \lambda_m sin(\theta) \\ v_b &= Ri_b + L\dot{i}_b + \omega \lambda_m sin(\theta - \frac{2\pi}{3}) \\ v_c &= Ri_c + L\dot{i}_c + \omega \lambda_m sin(\theta + \frac{2\pi}{3}) \end{aligned} \tag{3.3}$$

Where in equation 3.3 the back EMF generated on the stator are separately given with equation 3.4, are responsible for electromagnetic torque generation.

$$\begin{aligned} e_a &= \omega\lambda_m sin(\theta) \\ e_b &= \omega\lambda_m sin(\theta - \frac{2\pi}{3}) \\ e_c &= \omega\lambda_m sin(\theta + \frac{2\pi}{3}) \end{aligned} \tag{3.4}$$

Electromagnetic torque simplified as follows:

$$\begin{aligned} T_e &= \frac{1}{\omega}(E_a i_a + E_a i_a + E_a i_a) \\ &= \frac{P}{2}\lambda_m((i_a - \frac{1}{2}i_b - \frac{1}{2}i_b)sin(\theta) - \frac{\sqrt{3}}{2}(i_b - i_c)cos(\theta)) \end{aligned} \tag{3.5}$$

3.1.2 Stationary Orthogonal Reference Frame PMSM Modeling

These stationary model of a PMSM are in a distributed 3D reference frames, hence they are transformed onto another stationary orthogonal (α, β) reference frame.

$$\begin{aligned} v_\alpha &= Ri_\alpha + L\dot{i}_\alpha - \omega\lambda_m sin(\theta) \\ v_\beta &= Ri_\beta + L\dot{i}_\beta + \omega\lambda_m cos(\theta) \end{aligned} \tag{3.6}$$

$$T_e = \frac{P}{2}\lambda_m(-i_\alpha sin(\theta) + i_\beta cos(\theta)) \tag{3.7}$$

3.1.3 Rotary Orthogonal Reference Frame PMSM Modeling

The most common analysis is done using the d-q axis because it's applicable for both steady state and transient characteristic analysis. The d-q axis modeling is developed on the rotor refernce frame. At any time the rotating rotor d-axis makes an angle (θ_r) with the fixed stator phase-a axis and rotating stator magneto-motive force (MMF) makes an angle (α) with the rotor d-axis.

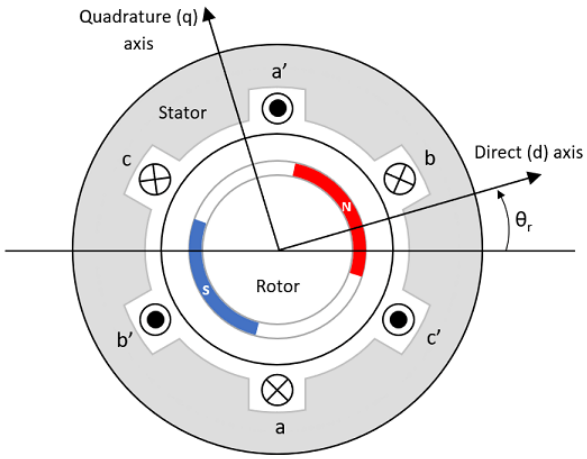

Figure 3.2: PMSM Construction with a Single Pole Pair on the Motor

$$\begin{aligned} v_d &= Ri_d + \frac{\partial \lambda_d}{\partial t} - \omega \lambda_q \\ v_q &= Ri_q + \frac{\partial \lambda_q}{\partial t} + \omega \lambda_d \end{aligned} \tag{3.8}$$

where the d-q axis linkage fluxes are given by equation 3.9 and the d-q axis inductances are the same in SPMSM i.e. $L_d = Lq$.

$$\begin{aligned} \lambda_d &= Li_d + \lambda_m \\ \lambda_q &= Li_q \end{aligned} \tag{3.9}$$

$$\begin{aligned} \dot{i}_d &= -\frac{R}{L} i_d + \omega i_q + \frac{v_d}{L} \\ \dot{i}_q &= -\frac{R}{L} i_q - \omega i_d - \frac{\lambda_m}{L}\omega + \frac{v_q}{L} \end{aligned} \tag{3.10}$$

The electromagnetic torque using the d-q axis variables is given by the following equation.

$$T_e = \frac{3}{2} p(\lambda_d i_q - \lambda_q i_d) \tag{3.11}$$

In order to produce maximum torque, to avoid reluctance effects and torque ripple, optimal operation is achieved by vector control, which ensures that the stator current space vector contains only a quadrature component by pushing d-axis current towards

zero $I_d = 0$. Thus the torque can be controlled directly by the quadrature current only. As a result the torque equation becomes:

$$T_e = \frac{3}{2} p \lambda_d i_q = \frac{3}{2} p \lambda_m i_q \tag{3.12}$$

And for all reference frame the electromechanical speed model is

$$\dot{\omega}_r = \frac{1}{J}(T_e - B\omega - T_L) = \frac{1}{J}(\frac{3}{2} p \lambda_m i_q - B\omega - T_L) \tag{3.13}$$

The angular speed for both electrical and mechanical positions is given by:

$$\begin{aligned} \omega &= \frac{d}{dt}\theta \qquad \omega_r &= \frac{d}{dt}\theta_r \\ \theta &= \frac{p}{2}\theta_r \qquad \omega &= \frac{p}{2}\omega_r \end{aligned} \tag{3.14}$$

Now lets concentrate on the state space model of the controlled state variables and control signals in the d-q axis representation. The first variable to-be controlled is the mechanical speed (ω_r) which is going to-be estimated through the Sliding Mode Observer (SMO). So the actual measured state space model will be as follows. The second variables are the d-q axis current variables so the complete state space model is given by equation 3.15.

$$\begin{aligned} \dot{\omega}_r &= \frac{3}{2J} p \lambda_m i_q - \frac{p}{2J} B \omega_r - \frac{1}{J} T_L \\ \dot{i}_d &= -\frac{R}{L} i_d + \frac{p}{2} \omega_r i_q + \frac{v_d}{L} \\ \dot{i}_q &= -\frac{R}{L} i_q - \frac{p}{2} \omega_r i_d - \frac{\lambda_m}{L} \frac{p}{2} \omega_r + \frac{v_q}{L} \end{aligned} \tag{3.15}$$

Chapter 4

Sensorless Permanent Magnet Synchronous Motor Speed Estimator and Controller Design

4.1 Speed Estimator Design in SPMSM

Designing an estimator for speed control in a PMSM is crucial for achieving accurate and efficient motor control. There are two commonly used methods for estimating position and speed of a surface mounted permanent magnet synchronous motor (SPMSM). These are encoder based and sensorless methods. The encoder based method utilizes an encoder directly attached to the motor shaft to directly measure position and speed. This method adds cost and complexity to the system and susceptible to mechanical wear and tear.

Hence, the sensorless method is going to-be used in this thesis research. It estimates position and speed without using a physical sensor. Instead, it relies on motor parameters and measurable quantities. It reduces cost, eliminates the need for additional hardware, and increases reliability. However,it is typically less accurate than encoder-based methods, especially at low speeds and under varying load conditions. There are different approaches for sensorless method: back EMF estimation, observer design, parameter identification, and feedback control.

In this thesis, analyzing the pros and cons of sensorless methods the back EMF based method is considered as a suitable sensorless control strategy for SPMSM [1]. However, this method is highly dependent and affected by the accuracy of the motor model. So, to overcome this dependency a more accurate nonlinear state space model of the motor and a nonlinear sliding mode observer (SMO) is applied. The SMO has good robustness against load disturbance and parameter perturbation.

However, the high-order harmonics in SMO are usually mixed with the back EMF signals. Hence, a low pass filter is needed to extract the fundamental back EMF signals. The introduction of filters cause phase delay and complicate the control system, which considerably deteriorates the dynamic performance of PMSM [18]. Another main issue of the traditional SMO is related to chattering caused by discrete time switching [19]. Several methods have been investigated to weaken the chattering phenomenon, thus an improved SMO based on the principle of super twisting algorithm is applied to estimate the rotor position and speed in this thesis.

The proposed SMO is shown in Figure 4.1. The rotor position and speed estimated by the observer are used for field orientation and closed loop control system design. The input of the observer is the given motor voltage recovered from the actually measured DC bus voltage and the duty cycle calculated from the space vector modulation module, which can partially eliminate the dead time effect of the inverter, so as to obtain more accurate actual given motor voltage.

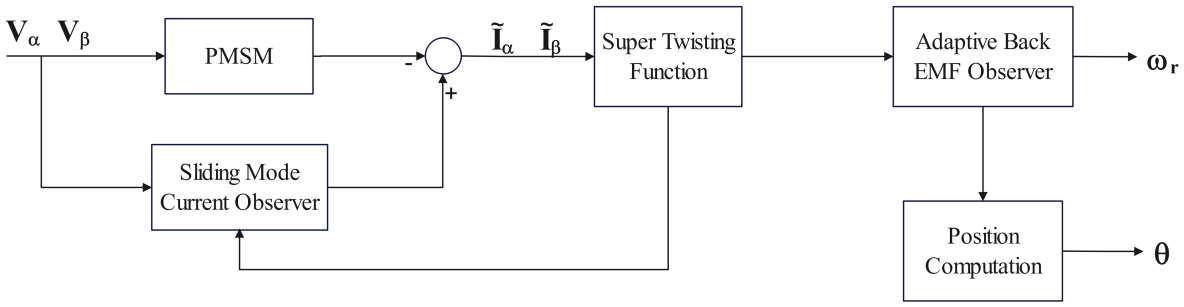

Figure 4.1: Block Diagram of SMO

The dynamics model of the SPMSM in the α-β frame is more convenient for the observer design based on the back-EMF signals [1, 28]. Thus, its mathematical modeling is given by equation 4.1.

$$\begin{aligned} \dot{i}_\alpha &= \frac{1}{L}(v_\alpha - Ri_\alpha - e_\alpha) \\ \dot{i}_\beta &= \frac{1}{L}(v_\beta - Ri_\beta - e_\beta) \end{aligned} \tag{4.1}$$

where i_α, i_β , v_α and v_β are the phase currents and voltages respectively in the α-β reference frame. L and R are the stator inductance and resistance respectively. e_α and e_β are back-EMF voltage signals in α-β reference frame, given by equation 4.2 [30].

$$\begin{aligned} e_\alpha &= -p\omega_r \Phi sin(\theta) \\ e_\beta &= p\omega_r \Phi cos(\theta) \end{aligned} \tag{4.2}$$

where ω_r is the mechanical angular speed, θ is the electrical angle of the motor, λ_m is the permanent magnet flux and p is the number of pole pairs. From the above equation it can be seen that the back-EMF voltage signals contain the rotor mechanical speed and position information. For the purpose of rotor position estimation, the super twisting high order sliding mode observer is designed as follows, where $\hat{i}_\alpha$ and $\hat{i}_\beta$ are the estimations of the phase currents in α-β frame, and v_1 and v_2 represent the observer control functions.

$$\begin{aligned} \dot{\hat{i}}_\alpha &= \frac{1}{L}(v_\alpha - R\hat{i}_\alpha - v_1) \\ \dot{\hat{i}}_\beta &= \frac{1}{L}(v_\beta - R\hat{i}_\beta - v_2) \end{aligned} \tag{4.3}$$

The super twisting algorithm for observer control functions is defined by equation 4.4.

$$\begin{aligned} v_1 &= k_1 |\tilde{i}_\alpha|^{\frac{1}{2}} sgn(\tilde{i}_\alpha) + \int k_2 sgn(\tilde{i}_\alpha) dt \\ v_2 &= k_1 |\tilde{i}_\beta|^{\frac{1}{2}} sgn(\tilde{i}_\beta) + \int k_2 sgn(\tilde{i}_\beta) dt \end{aligned} \tag{4.4}$$

where k_1 and k_2 are sliding mode gains, $k_1 > 0$ and $k_2 > 0$. The error equation for estimation of phase currents in α-β frame, $\tilde{i}_\alpha = \hat{i}_\alpha - i_\alpha$, and $\tilde{i}_\beta = \hat{i}_\beta - i_\beta$ are given by

equation 4.5.

$$\begin{aligned}\dot{\tilde{i}}_\alpha &= \frac{1}{L}(e_\alpha - R\tilde{i}_\alpha - v_1)\\ \dot{\tilde{i}}_\beta &= \frac{1}{L}(e_\beta - R\tilde{i}_\beta - v_2)\end{aligned} \tag{4.5}$$

These estimation errors of stator currents are selected to construct the sliding surface (s) of the super twisting algorithm as vectors of $s = [\tilde{i}_\alpha, \tilde{i}_\beta]^T$. Then the first time derivative of the sliding surface becomes:

$$\begin{aligned}\dot{\tilde{i}}_\alpha &= \frac{1}{L}(-k_1|\tilde{i}_\alpha|^{\frac{1}{2}}sgn(\tilde{i}_\alpha) - \int k_2 sgn(\tilde{i}_\alpha)dt) + \frac{R}{L}\tilde{i}_\alpha + \frac{e_\alpha}{L} + d_\alpha\\ \dot{\tilde{i}}_\beta &= \frac{1}{L}(-k_1|\tilde{i}_\beta|^{\frac{1}{2}}sgn(\tilde{i}_\beta) - \int k_2 sgn(\tilde{i}_\beta)dt) + \frac{R}{L}\tilde{i}_\beta + \frac{e_\beta}{L} + d_\beta\end{aligned} \tag{4.6}$$

where the terms $d_\alpha = \frac{R}{L}\tilde{i}_\alpha + \frac{e_\alpha}{L}$, $d_\beta = \frac{R}{L}\tilde{i}_\beta + \frac{e_\beta}{L}$ in equation 4.6 are considered as uncertainty. Compared with the standard form of the super twisting algorithm it's found that d_α and d_β are considered as the disturbance terms of the observer. Hence, once the system reaches the sliding surface, $\tilde{i}_\alpha = \tilde{i}_\beta = 0$ and $\dot{\tilde{i}}_\alpha = \dot{\tilde{i}}_\beta = 0$, the estimated back EMF signals expressed with equation 4.7.

$$\begin{aligned}e_\alpha &= k_1|\tilde{i}_\alpha|^{\frac{1}{2}}sgn(\tilde{i}_\alpha) + \int k_2 sgn(\tilde{i}_\alpha)dt\\ e_\beta &= k_1|\tilde{i}_\beta|^{\frac{1}{2}}sgn(\tilde{i}_\beta) + \int k_2 sgn(\tilde{i}_\beta)dt\end{aligned} \tag{4.7}$$

However, estimated signals of equation 4.7 still contain high frequency components. An adaptive observer instead of the traditional low pass filter is applied to extract the required back EMF signals. Since the change rate of the motor angular velocity is much lower than that of the stator current, it can be assumed that $\dot{\omega}_r = 0$. Then, the back EMF model of the PMSM can be expressed as in equation 4.8[20].

$$\begin{aligned}\dot{e}_\alpha &= -p\omega_r e_\beta\\ \dot{e}_\beta &= p\omega_r e_\alpha\end{aligned} \tag{4.8}$$

Based on equation 4.8, the adaptive observer is constructed as:

$$\begin{aligned}\dot{\hat{e}}_\alpha &= -p\hat{\omega}_r\hat{e}_\beta - k_3(\hat{e}_\alpha - e_\alpha)\\ \dot{\hat{e}}_\beta &= p\hat{\omega}_r\hat{e}_\alpha - k_4(\hat{e}_\beta - e_\beta)\\ \dot{\hat{\omega}}_r &= \frac{1}{p}[(\hat{e}_\alpha - e_\alpha)\hat{e}_\beta - (\hat{e}_\beta - e_\beta)\hat{e}_\alpha]\end{aligned} \tag{4.9}$$

where the observer gains are defined as, $k_3 > 0$ and $k_4 > 0$. The error equation of the adaptive observer is derived by subtracting equation 4.8 from equation 4.9 and given by equation 4.10.

$$\begin{aligned}\dot{\tilde{e}}_\alpha &= -p\tilde{\omega}_r\hat{e}_\beta - p\omega_r\tilde{e}_\beta - k_3\tilde{e}_\alpha\\ \dot{\tilde{e}}_\beta &= p\tilde{\omega}_r\hat{e}_\alpha - p\omega_r\tilde{e}_\alpha - k_4\tilde{e}_\beta\\ \dot{\tilde{\omega}}_r &= \frac{1}{p}(\tilde{e}_\alpha\hat{e}_\beta - \tilde{e}_\beta\hat{e}_\alpha)\end{aligned} \tag{4.10}$$

where $\tilde{e}_\alpha = \hat{e}_\alpha - e_\alpha$ and $\tilde{e}_\beta = \hat{e}_\beta - e_\beta$ are the back EMF estimation errors, and $\tilde{\omega}_r = \hat{\omega}_r - \omega_r$ are the speed estimation errors. Using equation 4.9, the rotor position can be estimated as follows.

$$\hat{\theta} = arctan(-\frac{\hat{e}_\alpha}{\hat{e}_\beta}) \tag{4.11}$$

4.2 SPMSM Controller Design

The state space model of the SPMSM is nonlinear, coupled, complex, multi-variable, and time varying system. So, to handle this problem a robust control scheme is needed. One of these controllers is the Sliding Mode Control (SMC) method. SMC is a class of variable structure system that targets decreasing the complexity of high-order systems to reduced-order state variables, defined as a sliding function and its derivative. SMC has advantageous for order reduction, disturbance rejection, insensitivity to parameter variations, decoupling design parameters and hence robust, and handles all system non-linearity and complexity.

SMC is one of the special backstepping feedback control systems because the uncer-

tainty and other disturbances are subtracted in the control design from the system. And the SMC utilizes high speed switching feedback control action. The application of SMC has disadvantages of: high level of chattering and not-robust against unmodeled dynamics (unmodeled uncertainty). Hence, to handle these problems there are lots of modification to the classical SMC design. These are adaptive SMC, fuzzy based SMC, higher order SMC, and fractional order sliding mode control (FOSMC). Therefore, FOSMC is going to-be designed and implemented in the following sections. The complete cascade control system for SPMSM is given by Figure 4.2.

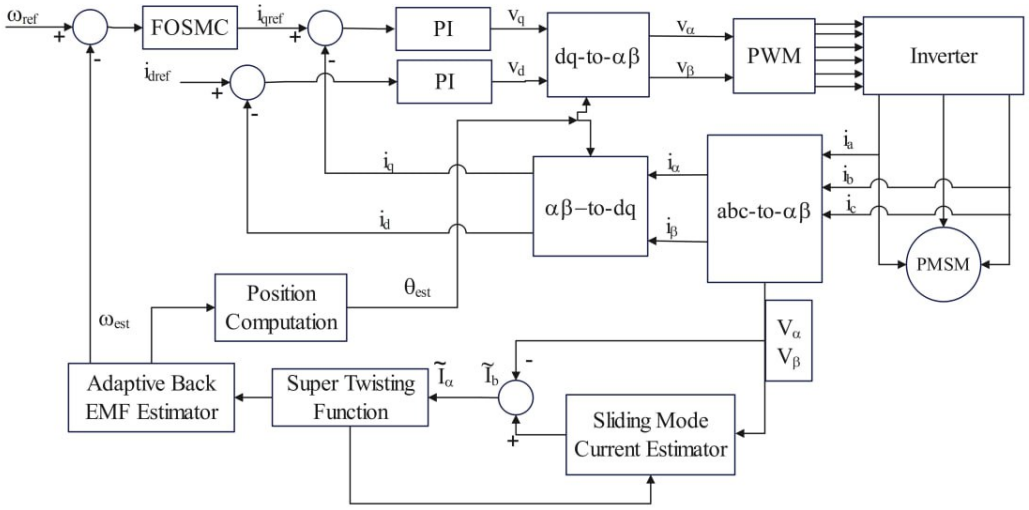

Figure 4.2: Cascade Control System Architecture

The complete mathematical model has two layers of control loops: speed and current control loops. The control algorithm should guarantee the precise tracking of the desired reference value of the controlled state variables. The controller design starts from the

following state space representation.

$$\begin{aligned}\dot{\omega}_r &= \frac{3}{2J}p\lambda_m i_q - \frac{p}{2J}B\omega_r - \frac{1}{J}T_L \\ \dot{i}_q &= -\frac{R}{L}i_q - \frac{p}{2}\omega_r i_d - \frac{\lambda_m}{L}\frac{p}{2}\omega_r + \frac{v_q}{L} \\ \dot{i}_d &= -\frac{R}{L}i_d + \frac{p}{2}\omega_r i_q + \frac{v_d}{L}\end{aligned} \tag{4.12}$$

SMC design has two phases of process or stages to be completed: sliding surface and control action design. The sliding surface is designed such that the system motion on the sliding mode can satisfy the design specifications. In this research the FOSMC is going to be designed, so the fractional orders of integration and derivatives orders are developed based on the principles of fractional order calculus 4.2.1. The control law is designed to drive the system state to the designed sliding surface and constrains the state to the surface subsequently [11]. There are two sets of control design equivalent and discontinuous (switching). The equivalent controllers try to drive the states from some initial condition onto the sliding surface, and dependent on the system dynamics. The discontinuous control is designed based on constant rate reaching law.

4.2.1 Fractional Order Calculus

Fractional calculus deals with derivatives and integrals of non-integer order [3, 15, 27, 31]. It extends the concepts of differentiation and integration to non-integer orders, which find applications in nonlinear, coupled, uncertain and complex mathematical models, sensorless PMSM sliding mode control. The sliding surface design given by Figure 4.3.

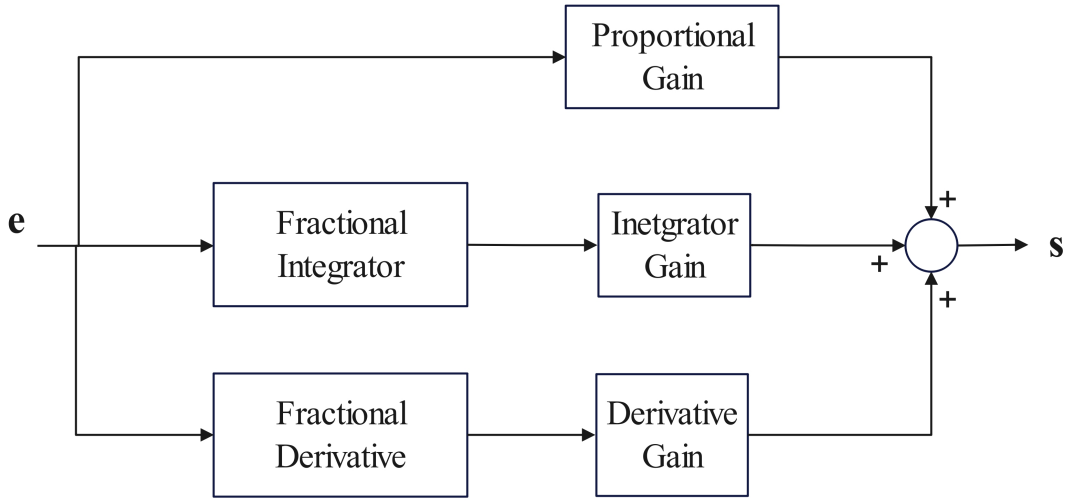

Figure 4.3: Block Diagram of Sliding Surface [3]

4.2.1.1 Fractional Integral

The fractional integral of a function $f(x)$ of order μ is denoted by $D^{\mu}f(x)$ and is defined as follows in equation 4.13.

$$D^{\mu}f(x) = \frac{1}{\Gamma(\mu)} \int_{a}^{x} (x-t)^{\mu-1} f(t)dt \tag{4.13}$$

where $\Gamma(\cdot)$ denotes the gamma function.

4.2.1.2 Fractional Derivative

The fractional derivative of a function $f(x)$ of order ϵ is denoted by $D^{\epsilon}f(x)$ and is defined as follows in equation 4.14.

$$D^{\epsilon}f(x) = \frac{1}{\Gamma(n-\epsilon)} \frac{d^n}{dx^n} \int_{a}^{x} (x-t)^{n-\epsilon-1} f(t)dt \tag{4.14}$$

where $n = \lceil \epsilon \rceil$ is the smallest integer greater than or equal to ϵ, and $\Gamma(\cdot)$ denotes the gamma function.

Fractional integrals and derivatives have the composition rules as follows [3, 27].

$$\begin{aligned} \frac{d^n}{dt^n}(D^\mu f(t)) &= D^{\mu+n} f(t) \\ \frac{d^n}{dt^n}(D^\epsilon f(t)) &= D^{\epsilon+n} f(t) \end{aligned} \tag{4.15}$$

4.2.2 FOSMC Design for Speed

Now lets start from speed controller design. Here the problem of controller design is about tracking some non zero reference speed. Hence the control design becomes a tracking problem. So let the desired mechanical speed of the motor be denoted with ω_{ref}, the actual mechanical speed be ω_r, and error be $e = \omega_{ref} - \omega_r$ then the error dynamics becomes:

$$\dot{e} = \dot{\omega}_{ref} - \dot{\omega}_r = \dot{\omega}_{ref} - \frac{3}{2J} p\lambda_m i_q + \frac{p}{2J} B\omega_r + \frac{1}{J} T_L \tag{4.16}$$

The speed is continuously manipulated with the q-axis current as can been seen from the above equation. So lets take the current i_q as the main controlling variable for speed and hence denote it with U_ω. Now the above error dynamic state space equation is rewritten using the notation U_ω as follows.

$$\dot{e} = \dot{\omega}_{ref} - \frac{3}{2J} p\lambda_m U_\omega + \frac{p}{2J} B\omega_r + \frac{1}{J} T_L \tag{4.17}$$

The fractional order sliding surface denoted by s_ω for speed control is defined as [15, 27]:

$$s_\omega = k_1 e + k_2 D^\mu e + k_3 D^\epsilon e \tag{4.18}$$

where k_1, k_2, k_3 are the positive coefficients of proportional, integral, and derivative gains respectively, D the integral and differential operator, and μ, and ϵ are the orders of integration and differentiation.

Taking the time derivative on both sides of equation 4.18 and applying the rules in

equation 4.15 yields the following sliding surface dynamics.

$$\dot{s}_\omega = k_1\dot{e} + k_2 D^{\mu+1}e + k_3 D^{\epsilon+1}e \tag{4.19}$$

Now based on the sliding surface and its dynamics both the equivalent and switching control laws are designed. The equivalent controller denoted with $U_{\omega_{eq}}$ is solved from equating the sliding dynamics equation 4.19 to zero. The discontinuous control is denoted with $U_{\omega_{dis}}$, and it's designed based on different laws of reaching conditions. Here in this research a exponential rate reaching law is adopted and designed. The exponential rate reaching law for speed discontinuous control is defined as in equation 4.20.

$$\dot{s}_\omega = -k_4 sgn(s_\omega) - k_5 s_\omega \tag{4.20}$$

The speed control law of the FOSMC can be designed combining the discontinuous and equivalent controllers, equating equation 4.19, and 4.20 and then solve for U_ω.

$$\begin{gathered} k_1\dot{e} + k_2 D^{\mu+1}e + k_3 D^{\epsilon+1}e = -k_4 sgn(s_\omega) - k_5 s_\omega \\ k_1(\dot{\omega}_{ref} - \frac{3}{2J}p\lambda_m U_\omega + \frac{p}{2J}B\omega_r + \frac{1}{J}T_L) = -k_2 D^{\mu+1}e - k_3 D^{\epsilon+1}e - k_4 sgn(s_\omega) - k_5 s_\omega \end{gathered} \tag{4.21}$$

$$U_\omega = \frac{2J}{3p\lambda_m k_1}(k_1(\dot{\omega}_{ref} + \frac{p}{2J}B\omega_r + \frac{1}{J}T_L) + k_2 D^{\mu+1}e + k_3 D^{\epsilon+1}e + k_4 sgn(s_\omega) + k_5 s_\omega) \tag{4.22}$$

Now the state space model of the speed including the control signal $I_q = U_\omega$ is given by equation 4.23.

$$\dot{\omega}_r = \frac{3}{2J}p\lambda_m U_\omega - \frac{p}{2J}B\omega_r - \frac{1}{J}T_L \tag{4.23}$$

4.2.3 PI Current Control Loops Design

In the inner-loop control there are two phases of control i.e. the q-axis and d-axis current control loops. Both are going to-be controlled in a separate fashion. The q-axis current control loop tries to make the actual q-axis current (i_q) follow the desired q-axis current ($i_{q_{ref}} = U_\omega$). Where as the d-axis current control loop tries to make the actual d-axis current toward zero asymptotically because in the design of the model it was assumed that the required d-axis current ($i_{d_{ref}}$) is zero.

Hence, let's start with the q-axis current (i_q) control. Let the desired q-axis current of the motor be denoted with $i_{q_{ref}}$, the actual current be i_q, and the error be $e = i_{q_{ref}} - i_q$ then the error dynamics are given by equation 4.24, where $i_{q_{ref}} = U_\omega$.

$$\dot{e} = \dot{i}_{q_{ref}} - \dot{i}_q = \dot{i}_{q_{ref}} + \frac{R}{L} i_q + \frac{p}{2}\omega_r i_d + \frac{\lambda_m}{L}\frac{p}{2}\omega_r - \frac{v_q}{L} \tag{4.24}$$

The q-axis current is continuously manipulated with the q-axis voltage as can be seen from the above equation. So let's take the voltage v_q as the main controlling variable for i_q and hence denote it with U_q. Here the desired d-axis current is set to zero for maximum flux and torque extraction, so the error and q-axis current dynamics simplified further as follows.

$$\begin{aligned} \dot{i}_q &= -\frac{R}{L} i_q - \frac{\lambda_m}{L}\frac{p}{2}\omega_r + \frac{U_q}{L} \\ \dot{e} &= \dot{i}_{q_{ref}} - \dot{i}_q = \dot{i}_{q_{ref}} + \frac{R}{L} i_q + \frac{\lambda_m}{L}\frac{p}{2}\omega_r - \frac{U_q}{L} \end{aligned} \tag{4.25}$$

The conventional PI controller for q-axis current control is defined as:

$$U_q = k_p e + k_i \int e\, dt \tag{4.26}$$

where k_p and k_i are the proportional and integral gains respectively.

Now let's go to the d-axis current control design. This is also known as regulation because the desired d-axis current is needed to be zero. So let the desired d-axis current of the motor be denoted with $i_{d_{ref}}$, the actual current be i_d, and error be $e = i_{d_{ref}} - i_d$

then the error dynamics are given by equation 4.27, where $i_{d_{ref}} = 0$.

$$\dot{e} = \dot{i}_{d_{ref}} - \dot{i}_d = \frac{R}{L} i_d - \frac{p}{2} \omega_r i_q - \frac{v_d}{L} \tag{4.27}$$

The d-axis current is continuously manipulated with the d-axis voltage as can be seen from the above equation. So let's take the voltage v_d as the main controlling variable for i_d and hence denote it with U_d. The conventional PI controller for d-axis current control is defined as in equation 4.28.

$$U_d = k_p e + k_i \int e \, dt \tag{4.28}$$

where k_p and k_i are the proportional and integral gains respectively.

4.3 Stability Analysis

Every controlled system must be ensured that its closed loop response is stable under the design conditions. One of the methods to prove the stability of the closed loop controlled system is the Lyapunov direct stability analysis technique. To analyze the stability of all designed controller lets start with the speed control loop and prove the stability conditions. Let the Lyapunov candidate function be selected as in equation 4.29.

$$V_{s_\omega} = \frac{1}{2} s_\omega^2 \tag{4.29}$$

Taking the first order time derivative of V_{s_ω} along the system trajectories, it results;

$$\begin{aligned}
\dot{V}_{s_\omega} &= s_\omega \dot{s}_\omega = s_\omega(k_1\dot{e} + k_2 D^{\mu+1}e + k_3 D^{\epsilon+1}e) \\
&= s_\omega(k_1(\dot{\omega}_{ref} - \frac{3}{2J}p\lambda_m U_\omega + \frac{p}{2J}B\omega_r + \frac{1}{J}T_L) + k_2 D^{\mu+1}e + k_3 D^{\epsilon+1}e) \\
&= s_\omega(-\frac{3k_1}{2J}p\lambda_m U_\omega + k_1\dot{\omega}_{ref} + \frac{k_1 p}{2J}B\omega_r + \frac{k_1}{J}T_L + k_2 D^{\mu+1}e + k_3 D^{\epsilon+1}e) \\
&= s_\omega(U_\omega - (1 + \frac{3k_1}{2J}p\lambda_m)U_\omega + k_1\dot{\omega}_{ref} + \frac{k_1 p}{2J}B\omega_r + \frac{k_1}{J}T_L + k_2 D^{\mu+1}e + k_3 D^{\epsilon+1}e) \\
&= s_\omega(U_\omega + d_V)
\end{aligned} \tag{4.30}$$

where $d_V = -(1+\frac{3k_1}{2J}p\lambda_m)U_\omega + k_1\dot{\omega}_{ref} + \frac{k_1 p}{2J}B\omega_r + \frac{k_1}{J}T_L + k_2 D^{\mu+1}e + k_3 D^{\epsilon+1}e$ is considered as the maximum strength value of the modeling within the Lyapunov function. But from the exponential rate reaching law of equation 4.20 we have the following relations for rewriting equation 4.30.

$$\begin{aligned}
\dot{V}_{s_\omega} &= s_\omega(-k_4 sgn(s_\omega) - k_5 s_\omega + d_V) \\
&= -k_4 s_\omega sgn(s_\omega) - k_5 s_\omega s_\omega + s_\omega d_V \\
&= -k_4|s_\omega| - k_5 s_\omega^2 + s_\omega d_V
\end{aligned} \tag{4.31}$$

According to stability theory of Lyapunov function, if $\dot{V}_{s_\omega} < 0$ and $V_{s_\omega} > 0$ are satisfied, the closed loop system is asymptotically stable, and then this can be proved as follows.

$$-k_4|s_\omega| - k_5 s_\omega^2 + s_\omega d_V < 0 \tag{4.32}$$

Here, the term $-k_5 s_\omega^2 < 0$ is absolutely deduced such that the gain k_5 has a positive value. Consequently, if $k_4 > d_V$ is satisfied, then $\dot{V}_{s_\omega} < 0$ is satisfied. Then, when time tends to reach infinity, s_ω goes to zero. Accordingly, we can easily conclude that the sliding surface will be bounded in finite time for positive gain values of the exponential reaching law design.

Now the second phase of closed loop stability analysis is done for the current control loops in a similar fashion. The Lyapunov functions for the q-axis and d-axis current

control loops selected as $V_{s_q} = \frac{1}{2}s_q^2$, and $V_{s_d} = \frac{1}{2}s_d^2$ respectively. Taking similar procedures the stability of individual current control loops is proved through designing a control parameter as $k_p > 0$, and $k_i > 0$ such that the switching gains should have much enough strength to cancel out the uncertainty existing though each control channel.

Finally, the complete closed loop control system stability can be proved by selecting the composite Lyapunov function as in equation 4.33.

$$V_s = V_{s_\omega} + V_{s_q} + V_{s_d} = \frac{1}{2}s_\omega^2 + \frac{1}{2}s_q^2 + \frac{1}{2}s_d^2 \tag{4.33}$$

Chapter 5

Simulation Results and Analysis

5.1 Synchronous Motor Specification

In this thesis a special type of PMSM which is verified in MATLAB simscape electrical power systems is under study for applying a closed-loop speed, current control, speed estimation, and position estimation. The three-phase motor rated 1.1 kW, 220 V, 3000 rpm was fed by a PWM inverter. The PWM inverter is built entirely with standard simulink® blocks. Its output goes through controlled voltage source blocks before being applied to the PMSM block's stator windings. All other detail specifications of the motor is discussed in Table 5.1.

Table 5.1: Surface Mounted Permanent Magnet Synchronous Motor Parameters

Parameter	**Symbol**	**Value**	**SI unit**
Nominal DC voltage	U	310	V
Stator resistance	R	2.875	Ω
Cross d-axis inductance	L_d	1.53	mH
Cross q-axis inductance	L_q	1.53	mH
Permanent magnet chain flux	ψ_f	0.175	Wb
Moment of inertia	J	0.0008	Kg m2

Continued on next page

Table 5.1 – continued from previous page

Viscous damping coefficient	B	0.000	N m sec /rad
Number of pole pairs	p	4	-

Two control loops are used. The inner loop regulates the motor's stator d-axis current and controls the motor's stator q-axis motor to a certain value. The outer loop controls the motor's speed towards some desired reference speed.

The effectiveness of the proposed control and observer methodology was demonstrated using the simulation results based on a sensorless PMSM drive system which was built using MATLAB simulink. In the simulation setup the SPMSM system with its electrical and mechanical dynamics along with the associated motor and drive parameters were modeled. FOSMC was set in MATLAB as the primary control strategy for the motor's speed, and PI current control loops take the leveraging fractional calculus-based approach of speed control to enhance control performance. The speed estimator was also presented and compared with the actual speed measurement values from the motor.

The nonlinear model and controller were verified, and tested through different simulation scenarios;in the presence of external input disturbances, external load variation, and parameter variation. The nominal simulation was performed first in the absence of input disturbance, and parameter variation however, in the presence of standard nominal load torque applied to the shaft of a PMSM. The nominal load torque applied to the shaft of a permanent magnet synchronous machine in a Simulink simulation is typically calculated based on the machine's rated power and speed. This is approached through equation 5.1.

$$T = \frac{P}{\omega} \tag{5.1}$$

where (ω) is the rated angular velocity in radians per second (rad/s), (P) is the rated power of the machine in watts (W) or kilowatts (kW) and (T_L) is the nominal load torque in Newton meter (N.m). Now let's calculate the actual value of nominal load torque referring equation 5.1.

$$T = \frac{P}{\omega} = \frac{1100}{\frac{3000*2\pi}{60}} \frac{\text{Watt}}{\text{rad/sec}} = \frac{1100}{314.16} \approx 3.5 \text{ Nm} \tag{5.2}$$

Therefore, the nominal load torque to be applied in the nominal simulation for the PMSM is slightly lower than 3.5 Nm, and taken as 3 Nm for the safety pre-condition. Finally, the effect of the load variation, input disturbance, and parameter variation introduced for verification of designed controller robustness.

The simulation was performed in different working ranges of speed from rated to low speed operations. This is demonstrated in the following sections with graphical plots of results. In the nominal simulation scenario for a SPMSM, the motor model, incorporating detailed equations for electrical and mechanical behavior along with accurate parameterization, is combined with a sophisticated control system employing FOSMC strategy. Simulations are conducted in a MATLAB environment with appropriate solver settings and a representative mechanical load. Through steady-state and transient testing scenarios, the motor's performance in maintaining desired speed is evaluated.

5.2 Nominal Simulation Scenario at 300 rad/sec

The motor simulated near it's rated speed of 300 rad/sec and the following results were recorded and demonstrated with the subsequent graph plots.

Controller Gains	k_1	k_2	k_3	k_4	k_5	μ	ϵ	$k_{p_{I_q}}$	$k_{i_{I_q}}$	$k_{p_{I_d}}$	$k_{i_{I_d}}$
Values	10	50	0.3	0.15	25	-0.01	0.01	2	300	1	300

Table 5.2: Controller Gains for 300 rad/sec Reference Speed

Estimator Gains	K_1	K_2	K_3	K_4
Values	500	0.1	170	170

Table 5.3: Estimator Gains for 300 rad/sec Reference Speed

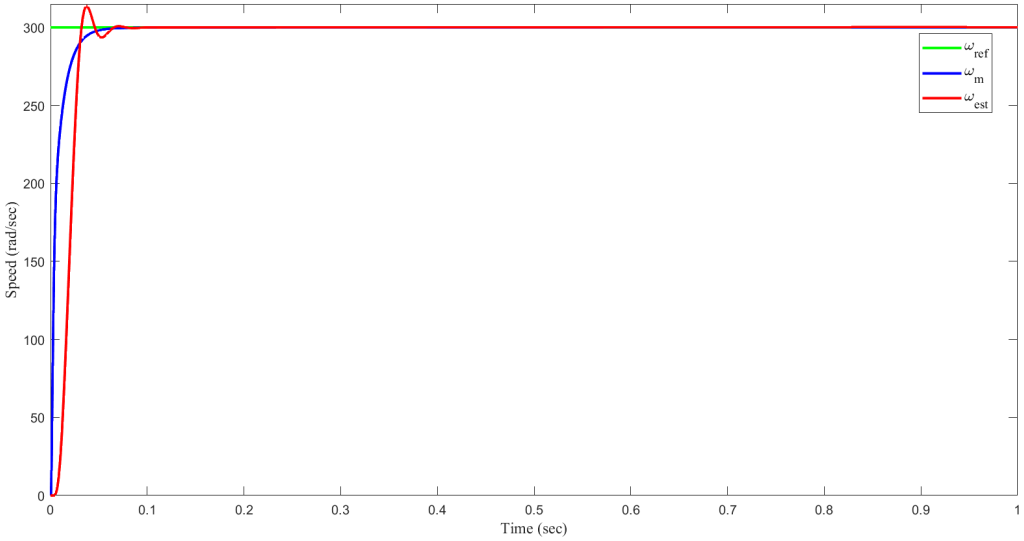

Figure 5.1: Speed Tracking

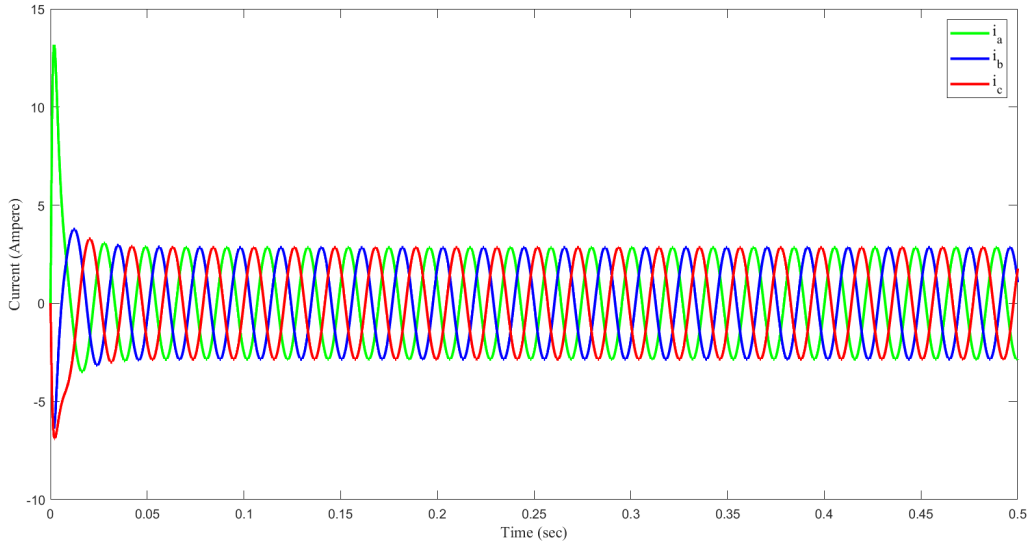

Figure 5.2: Three Phase Current Output of Motor

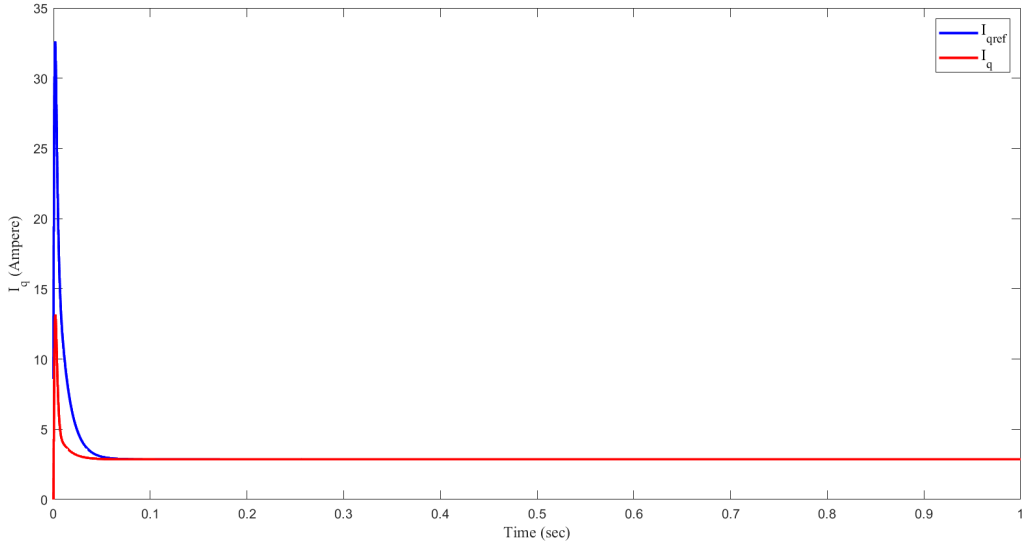

Figure 5.3: Current Tracking Along q-axis

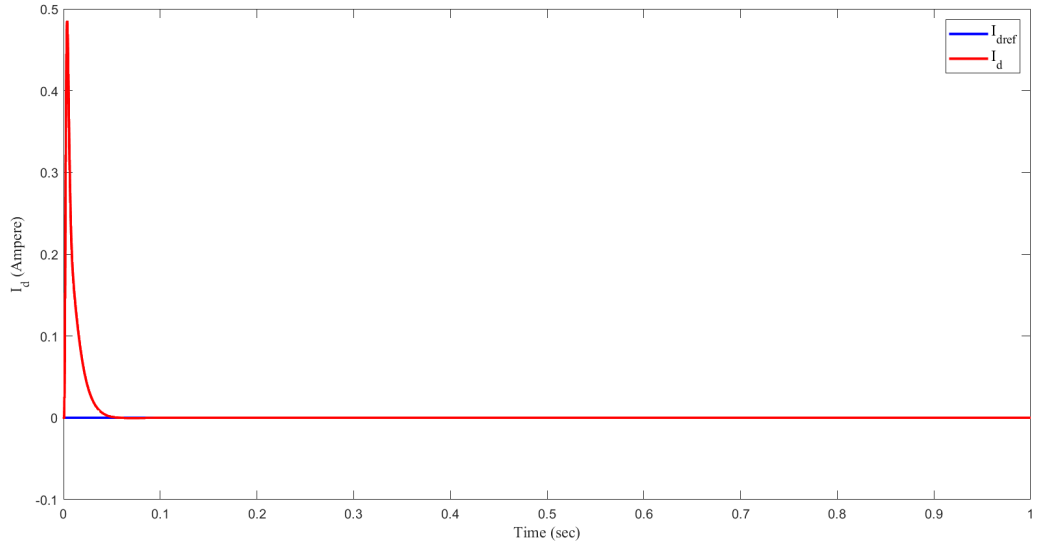

Figure 5.4: Current Tracking Along d-axis

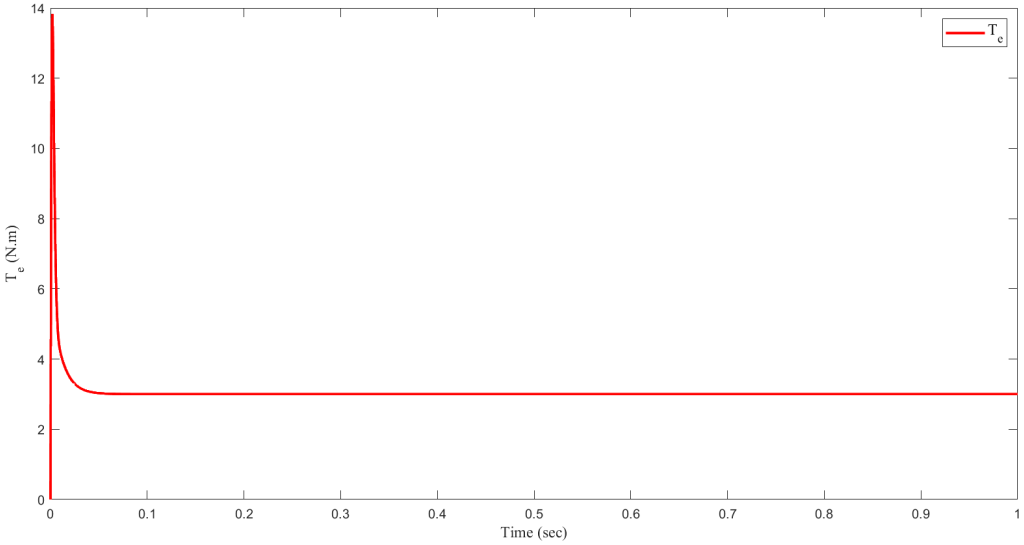

Figure 5.5: Electrical Torque of the Motor

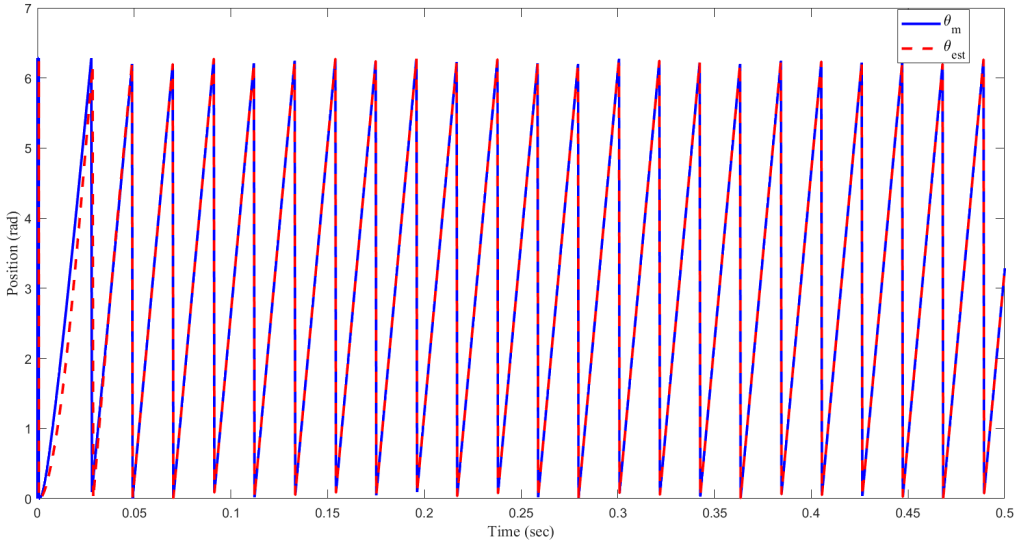

Figure 5.6: Position Measurement and Estimation

5.3 Nominal Simulation Scenario at 200 rad/sec

In order to evaluate the performance of the proposed control strategy under nominal external load the reference speed of 200 rad/sec tracking simulations performed as follows.

Controller Gains	k_1	k_2	k_3	k_4	k_5	μ	ϵ	$k_{p_{I_q}}$	$k_{i_{I_q}}$	$k_{p_{I_d}}$	$k_{i_{I_d}}$
Values	10	50	0.3	0.15	25	-0.01	0.01	2	300	1	300

Table 5.4: Controller Gains for 200 rad/sec Reference Speed

Estimator Gains	K_1	K_2	K_3	K_4
Values	500	0.1	170	170

Table 5.5: Estimator Gains for 200 rad/sec Reference Speed

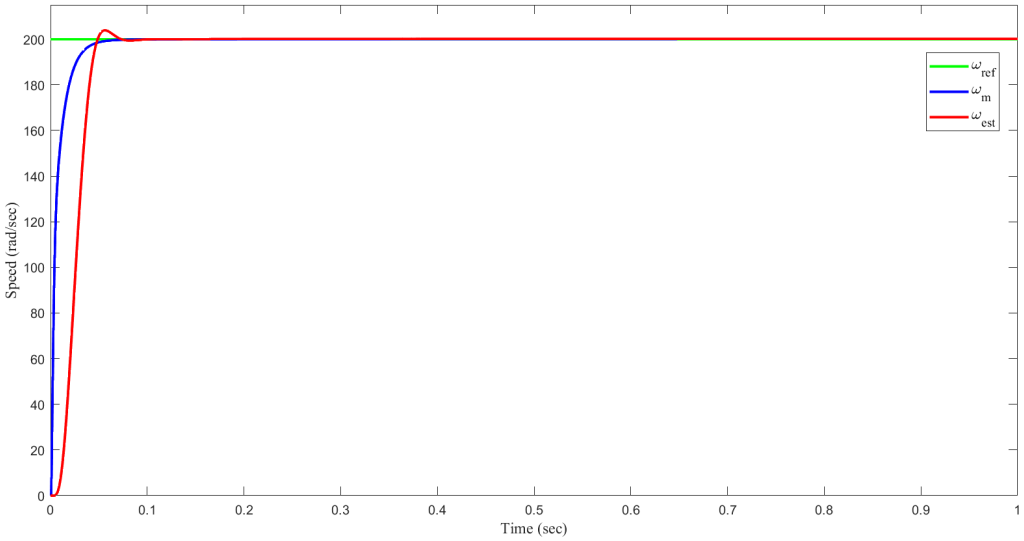

Figure 5.7: Speed Tracking Under Load Torque

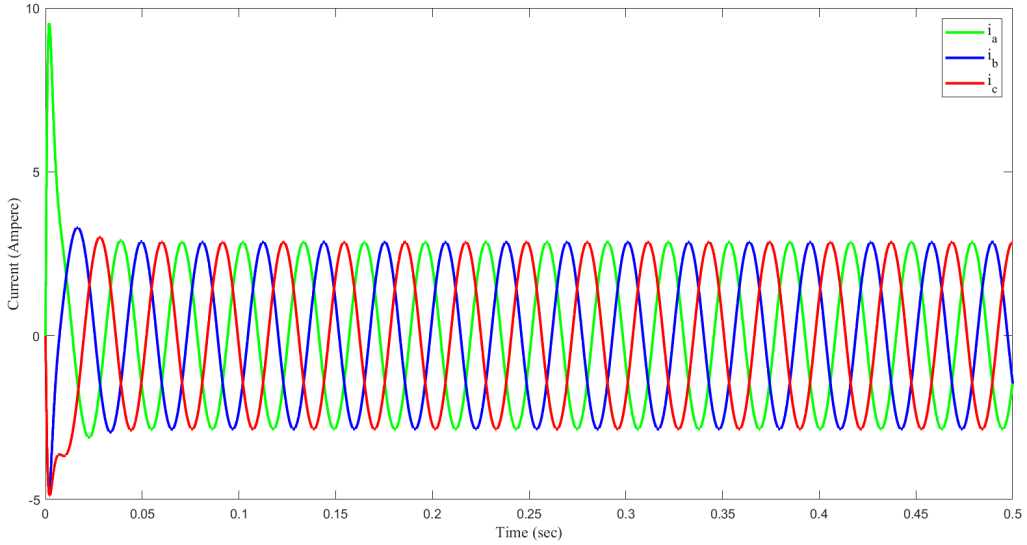

Figure 5.8: Three Phase Current Output of Motor Under Load Torque

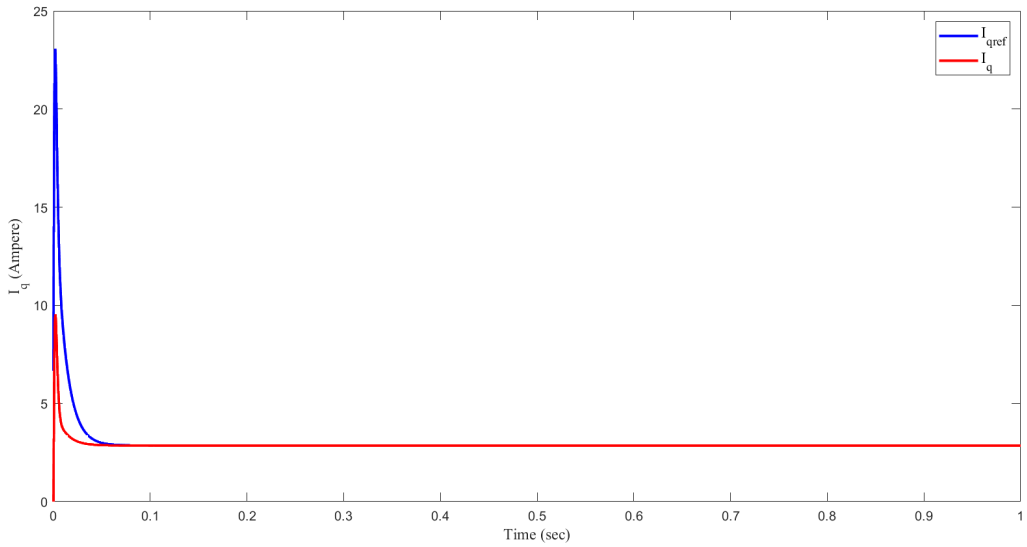

Figure 5.9: Current Tracking Along q-axis Under Load Torque

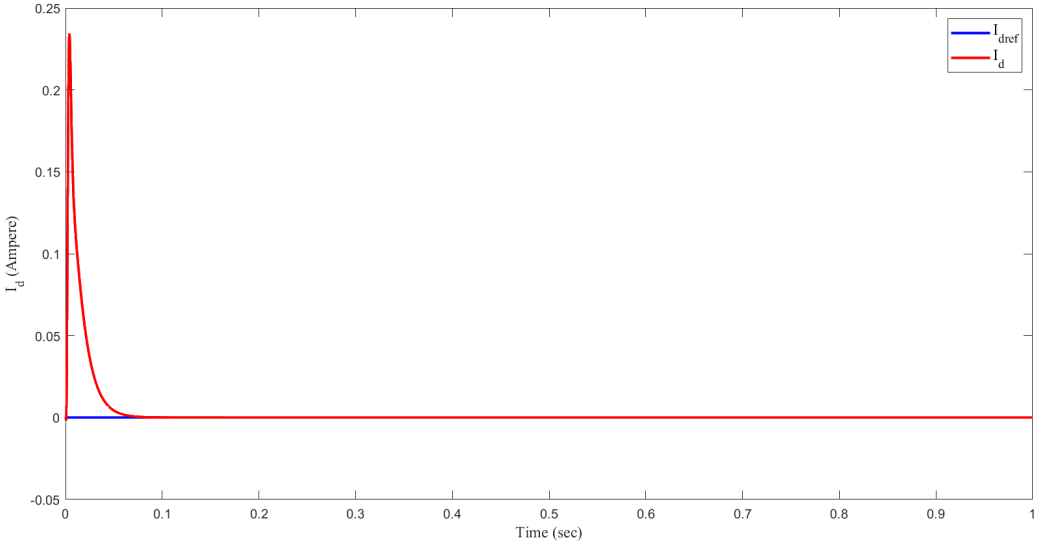

Figure 5.10: Current Tracking Along d-axis Under Load Torque

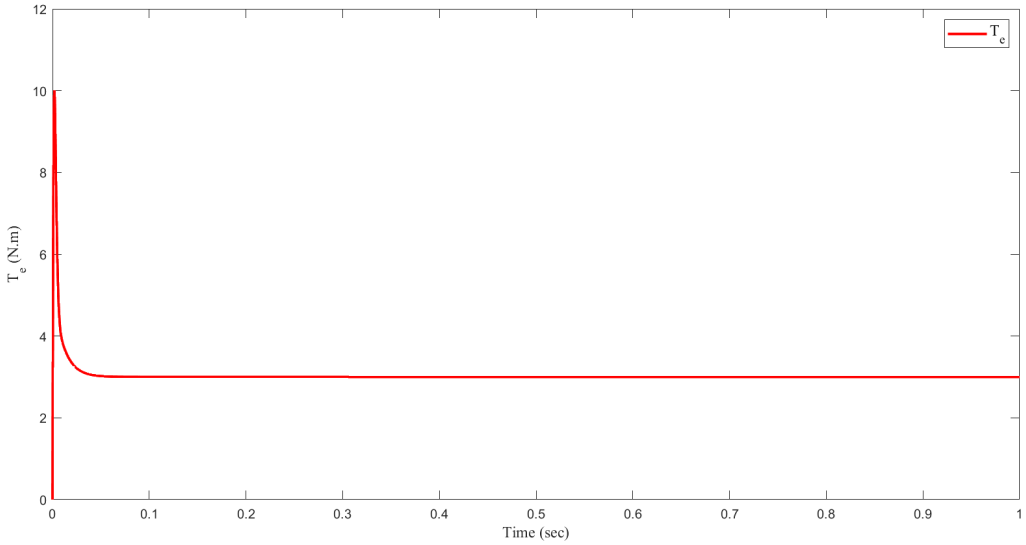

Figure 5.11: Electrical Torque of the Motor Under Load Torque

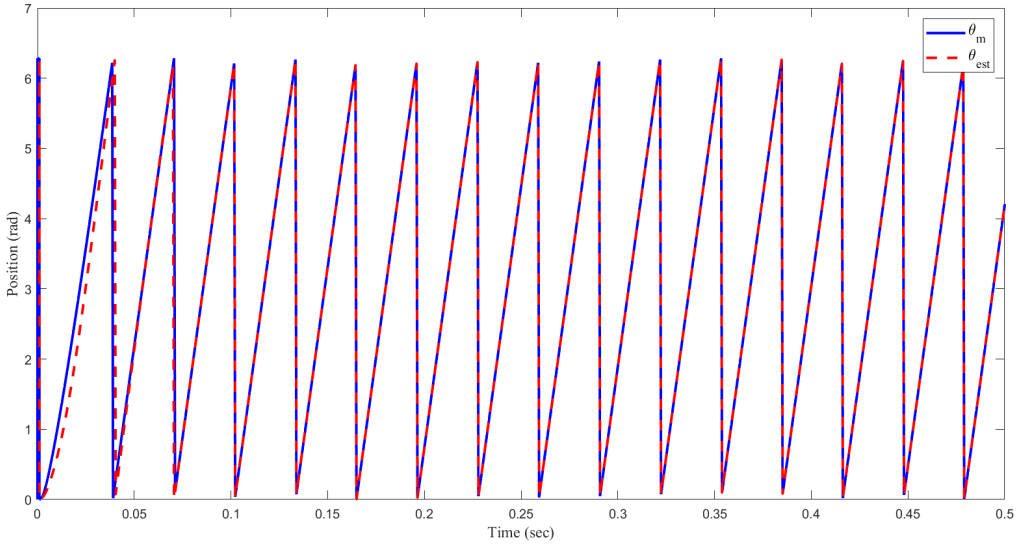

Figure 5.12: Position Measurement and Estimation Under Load Torque

5.4 Nominal Simulation Scenario at 100 rad/sec

In most literature's the 100 rad/sec reference speed is preferred for simulation as an average speed range of lower range operation, this is verified in the following figures.

Controller Gains	k_1	k_2	k_3	k_4	k_5	μ	ϵ	$k_{p_{I_q}}$	$k_{i_{I_q}}$	$k_{p_{I_d}}$	$k_{i_{I_d}}$
Values	10	50	0.3	0.15	25	-0.01	0.01	2	300	1	300

Table 5.6: Controller Gains for 100 rad/sec Reference Speed

Estimator Gains	K_1	K_2	K_3	K_4
Values	500	0.1	170	170

Table 5.7: Estimator Gains for 100 rad/sec Reference Speed

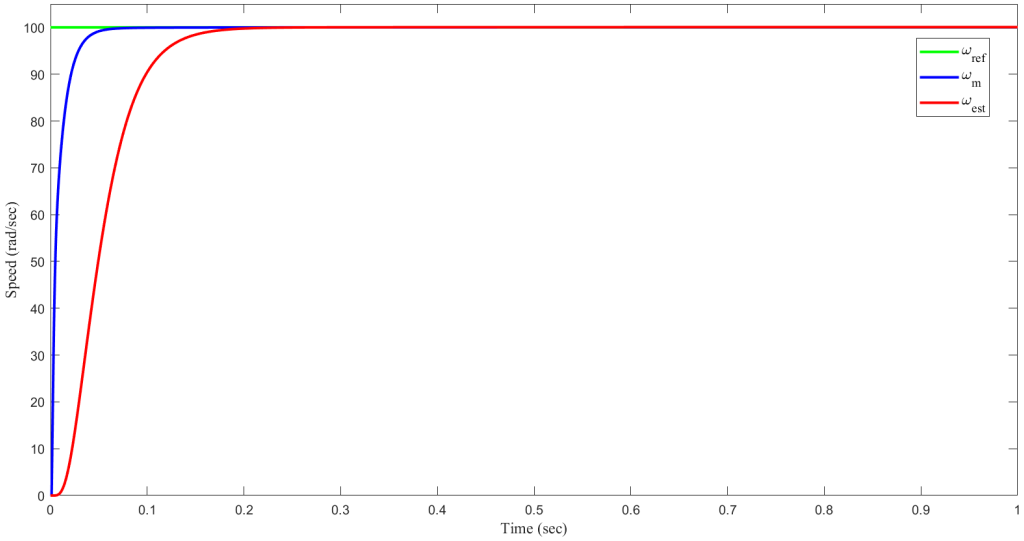

Figure 5.13: Speed Tracking Under Load Torque

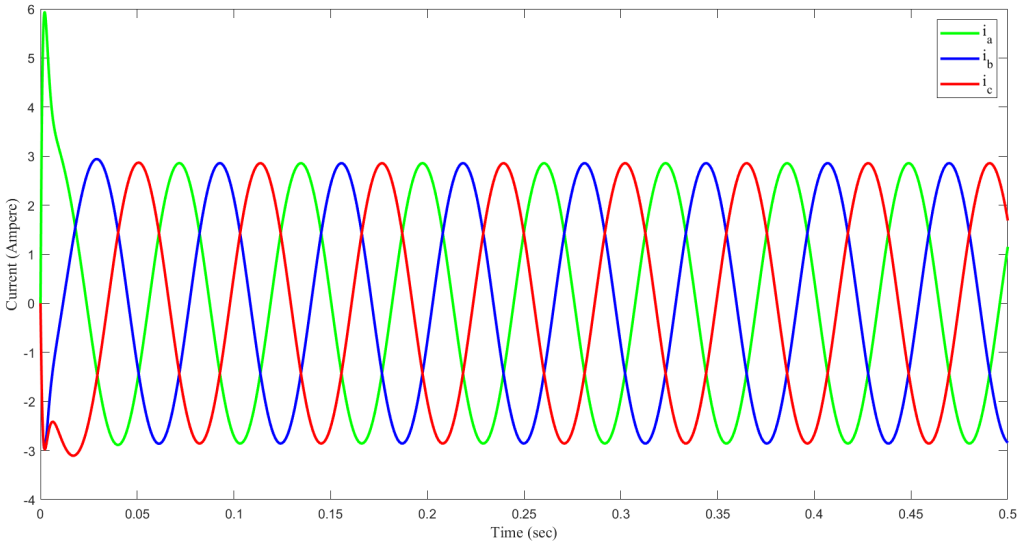

Figure 5.14: Three Phase Current Output of Motor Under Load Torque

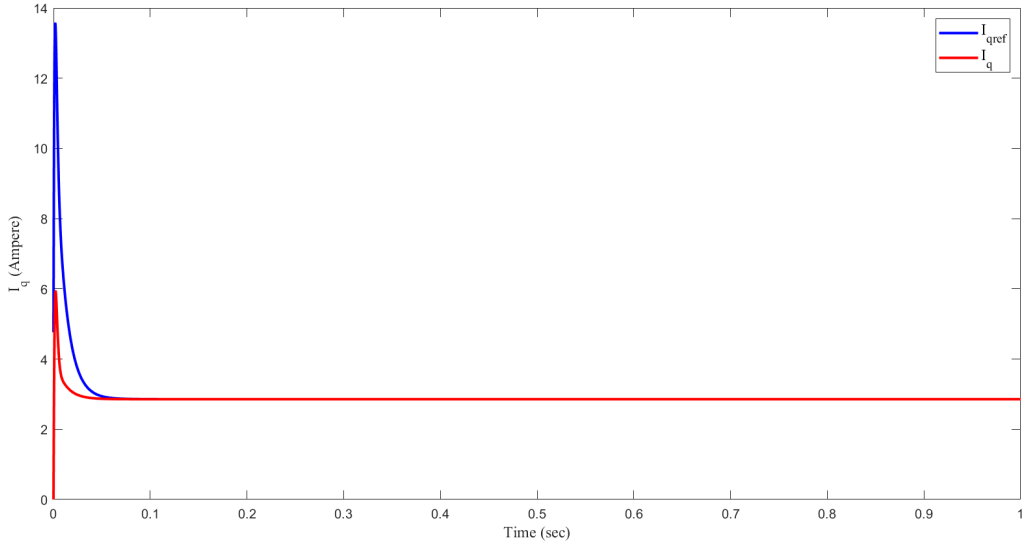

Figure 5.15: Current Tracking Along q-axis Under Load Torque

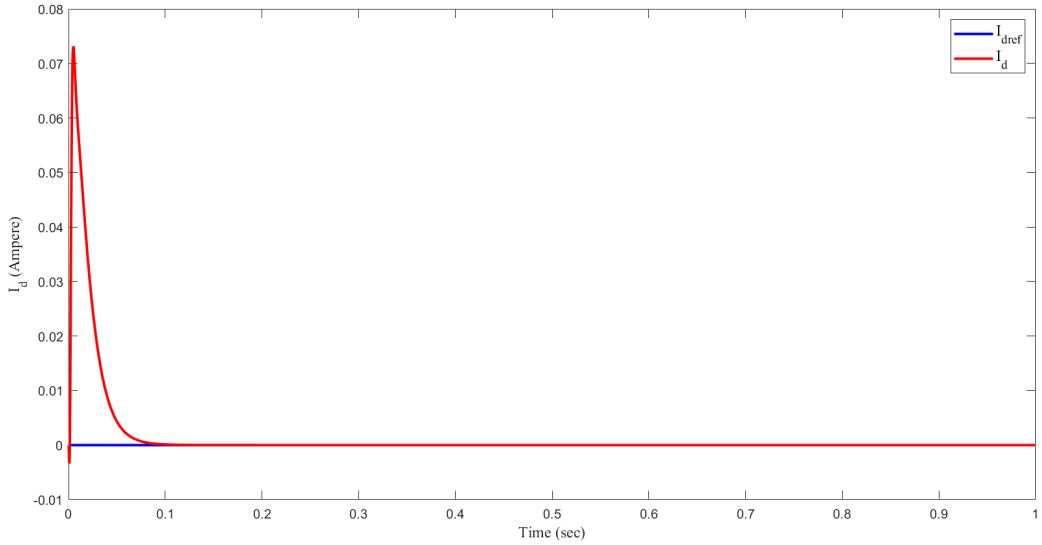

Figure 5.16: Current Tracking Along d-axis Under Load Torque

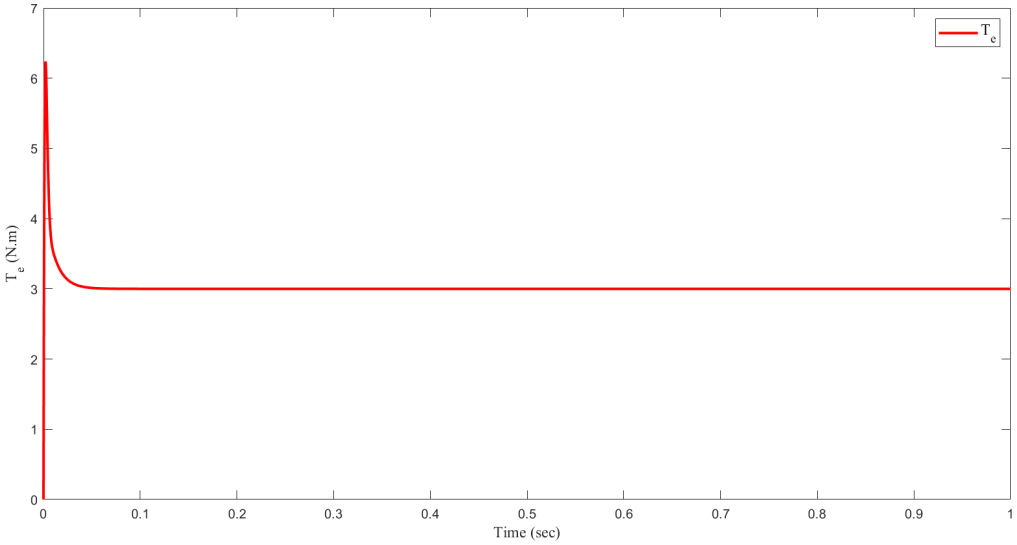

Figure 5.17: Electrical Torque of the Motor Under Load Torque

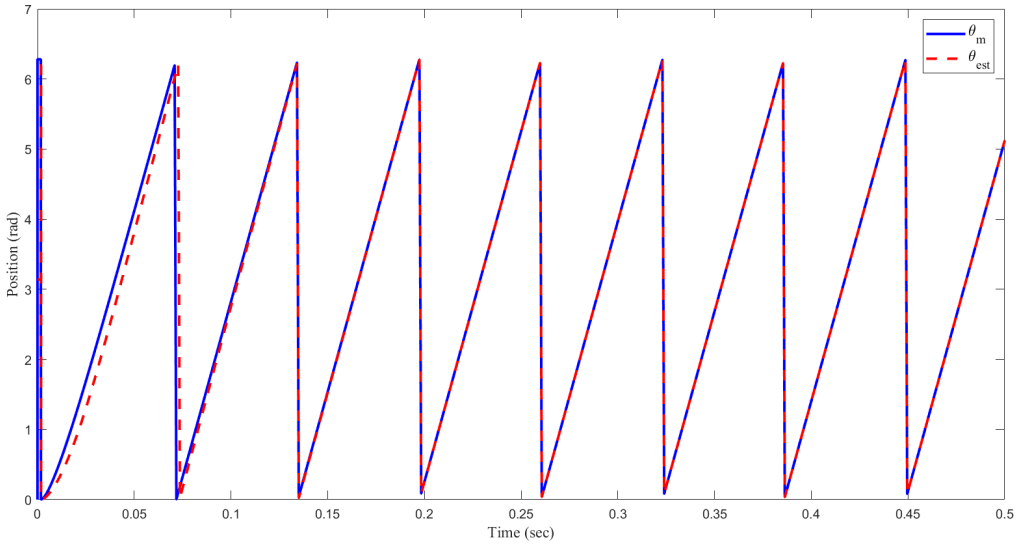

Figure 5.18: Position Measurement and Estimation Under Load Torque

5.5 Nominal Simulation Scenario at 63 rad/sec

This reference speed is called a 20% value of the nominal speed which is usually called the upper bound of the lower speed operating region of the PMSM.

Controller Gains	k_1	k_2	k_3	k_4	k_5	μ	ϵ	$k_{p_{I_q}}$	$k_{i_{I_q}}$	$k_{p_{I_d}}$	$k_{i_{I_d}}$
Values	1.5	2	0.3	10	20	-0.01	0.01	100	500	100	500

Table 5.8: Controller Gains for 63 rad/sec Reference Speed

Estimator Gains	K_1	K_2	K_3	K_4
Values	500	200	50	50

Table 5.9: Estimator Gains for 63 rad/sec Reference Speed

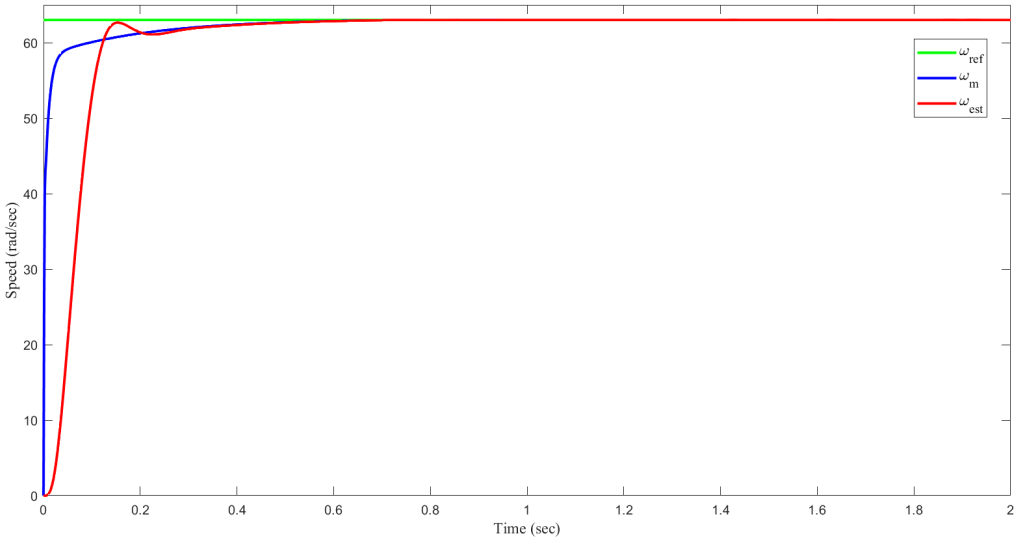

Figure 5.19: Speed Tracking Under Load Torque

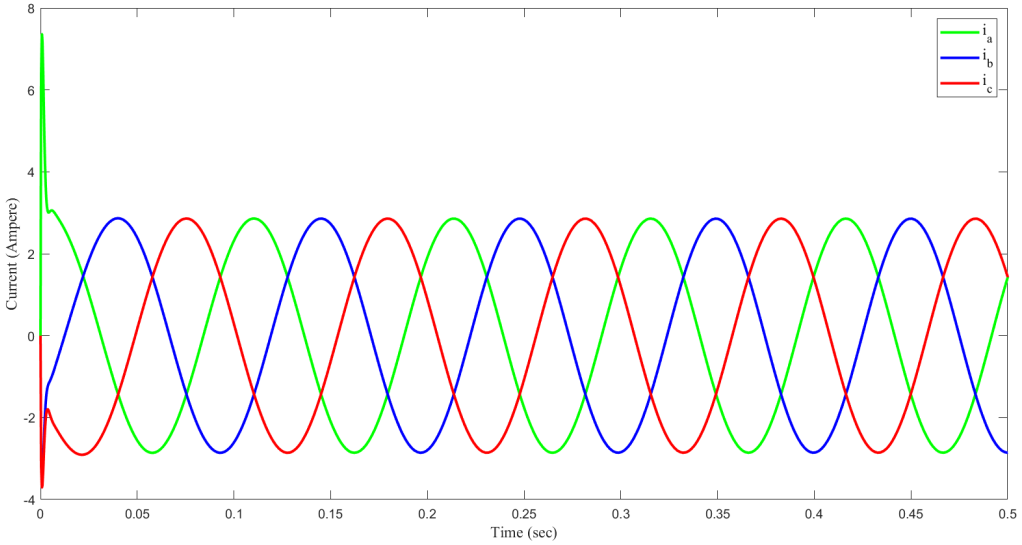

Figure 5.20: Three Phase Current Output of Motor Under Load Torque

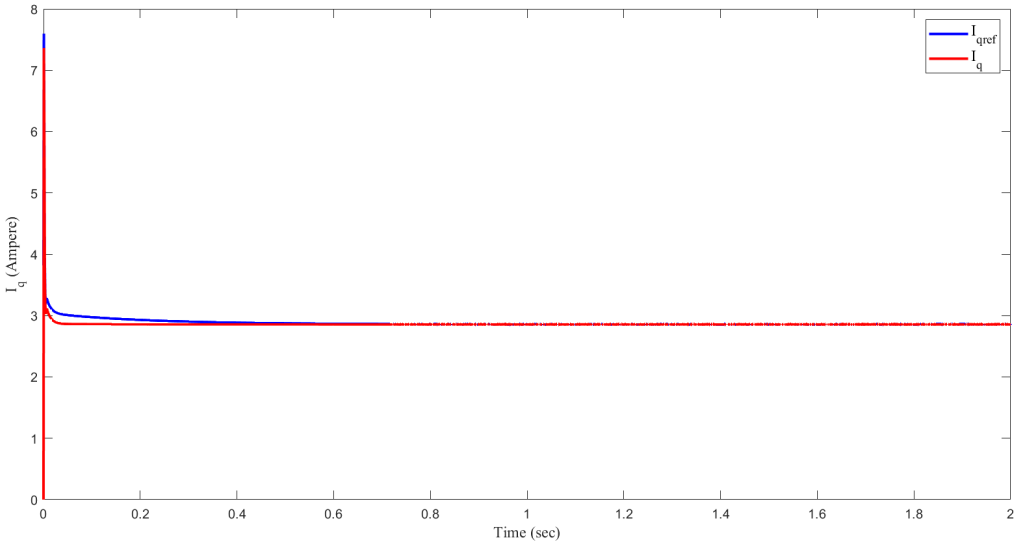

Figure 5.21: Current Tracking Along q-axis Under Load Torque

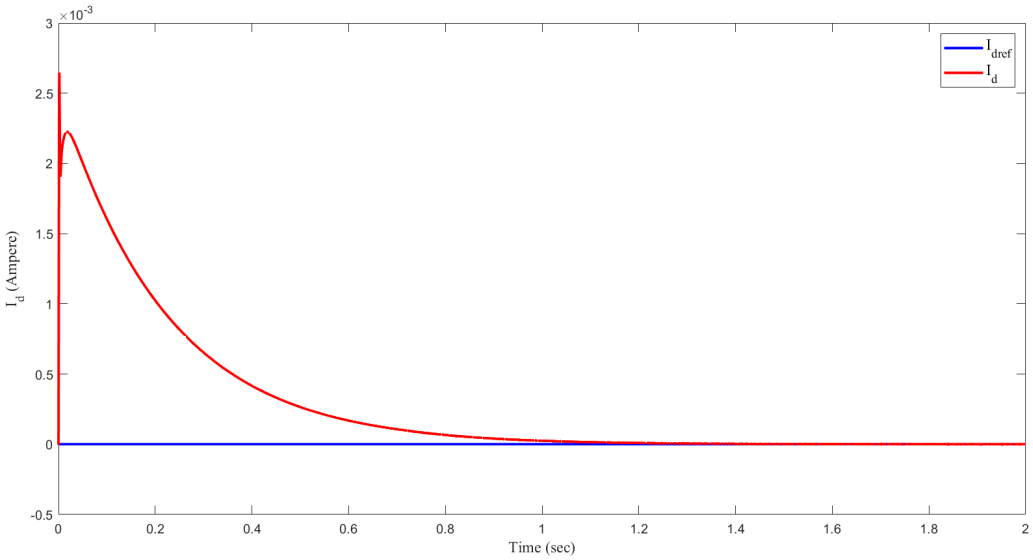

Figure 5.22: Current Tracking Along d-axis Under Load Torque

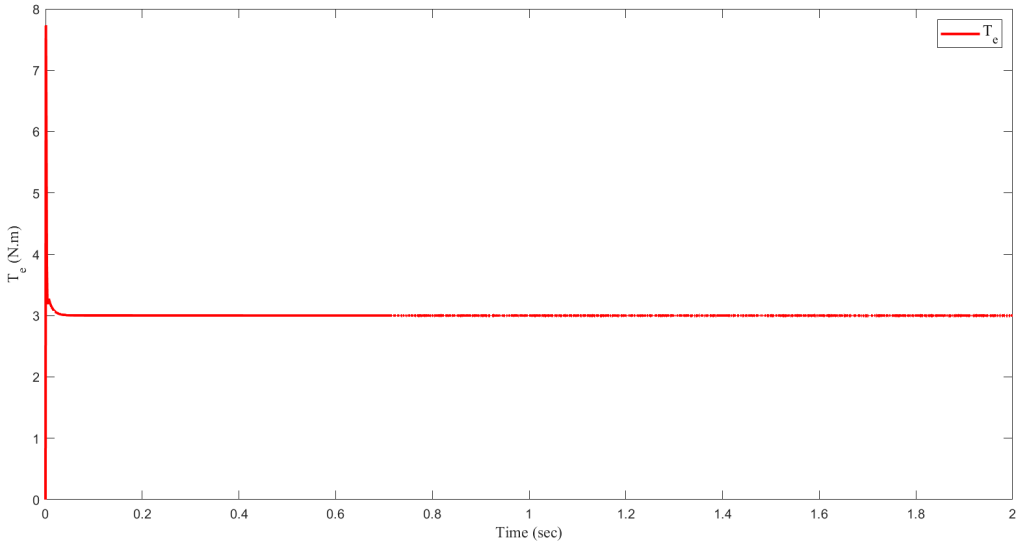

Figure 5.23: Electrical Torque of the Motor Under Load Torque

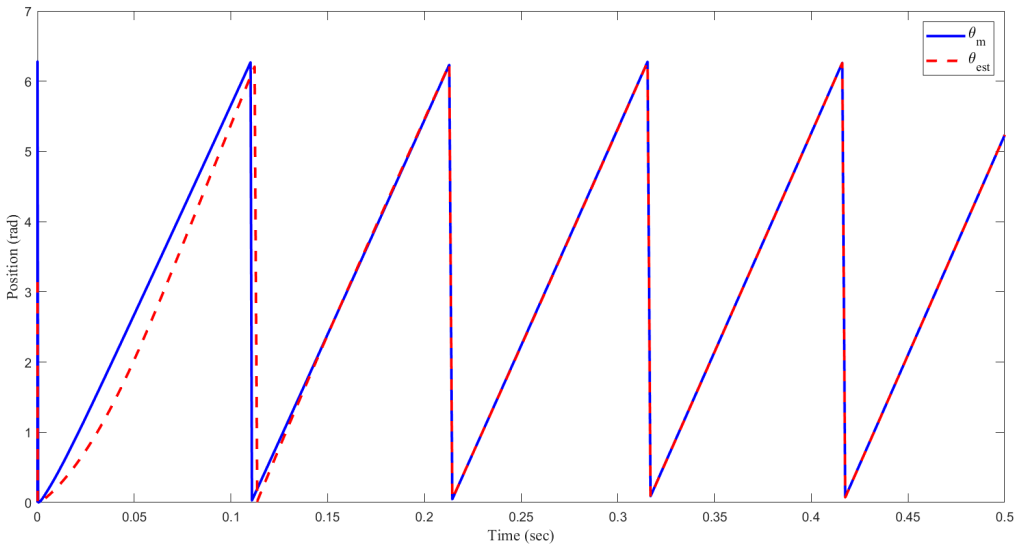

Figure 5.24: Position Measurement and Estimation Under Load Torque

5.6 Nominal Simulation Scenario at 31.5 rad/sec

The nominal lower bound of lower speed operating range of this PMSM is taken as a 10% of its rated speed which is 31.5 rad/sec.

Controller Gains	k_1	k_2	k_3	k_4	k_5	μ	ϵ	$k_{p_{I_q}}$	$k_{i_{I_q}}$	$k_{p_{I_d}}$	$k_{i_{I_d}}$
Values	1.5	2	0.3	10	20	-0.01	0.01	100	500	100	500

Table 5.10: Controller Gains for 31.5 rad/sec Reference Speed

Estimator Gains	K_1	K_2	K_3	K_4
Values	500	100	50	50

Table 5.11: Estimator Gains for 31.5 rad/sec Reference Speed

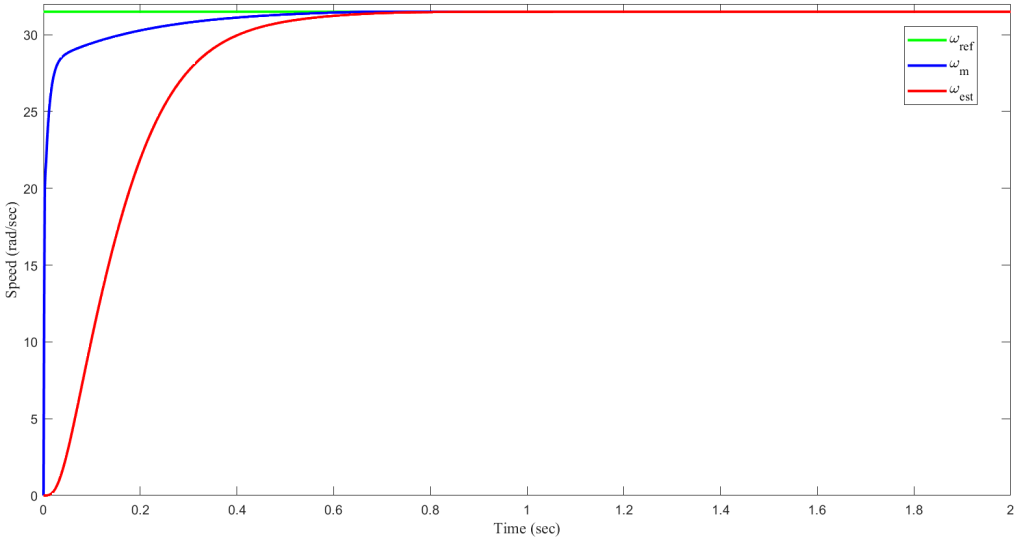

Figure 5.25: Speed Tracking Under Load Torque

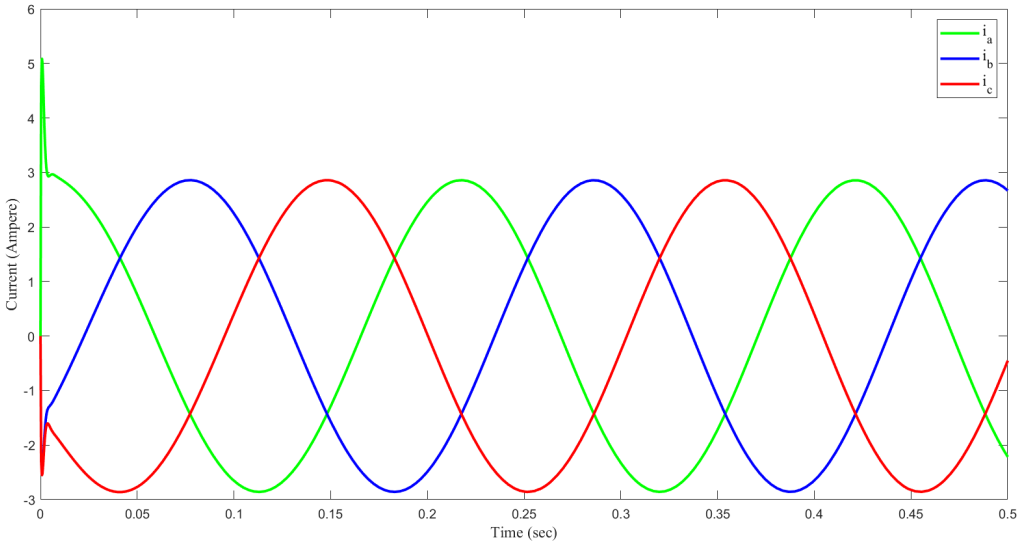

Figure 5.26: Three Phase Current Output of Motor Under Load Torque

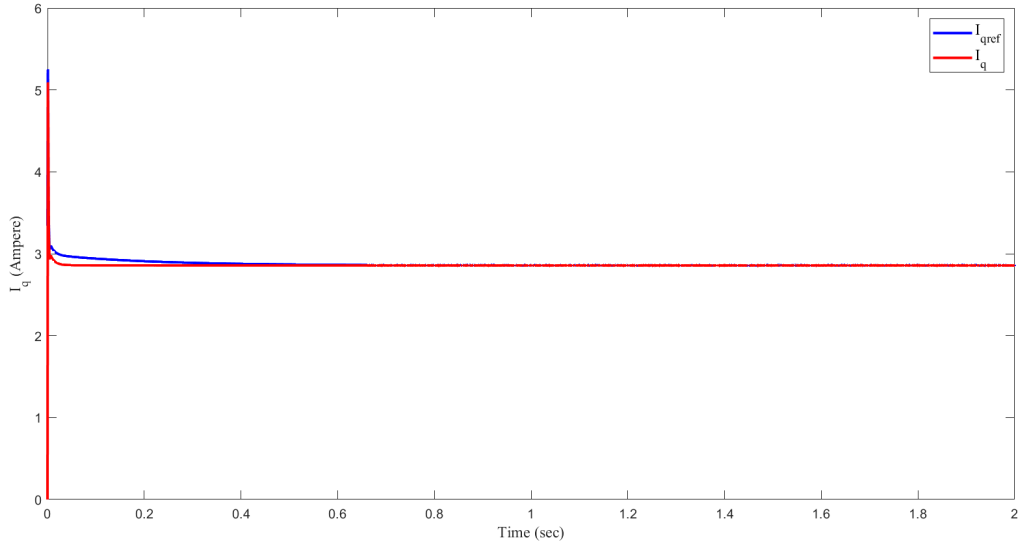

Figure 5.27: Current Tracking Along q-axis Under Load Torque

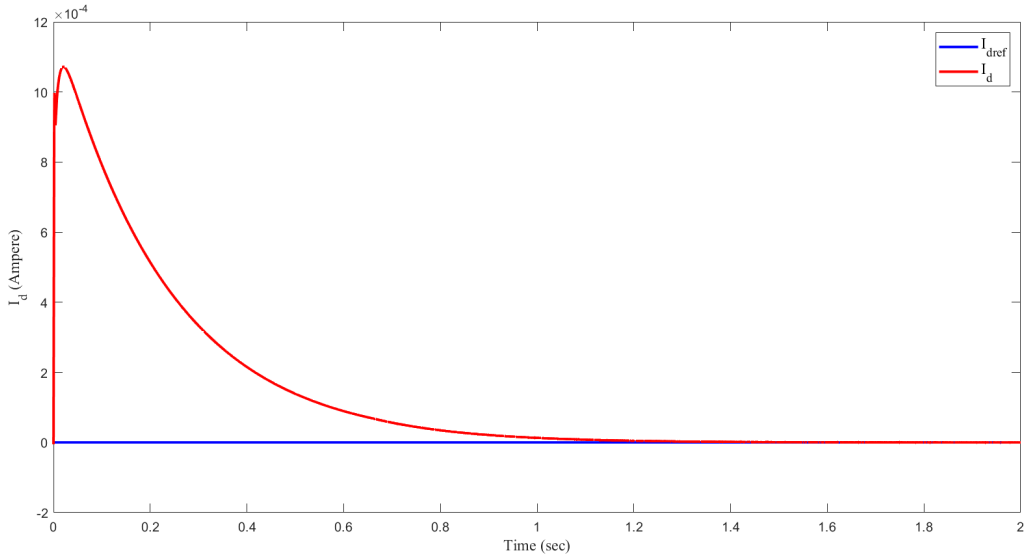

Figure 5.28: Current Tracking Along d-axis Under Load Torque

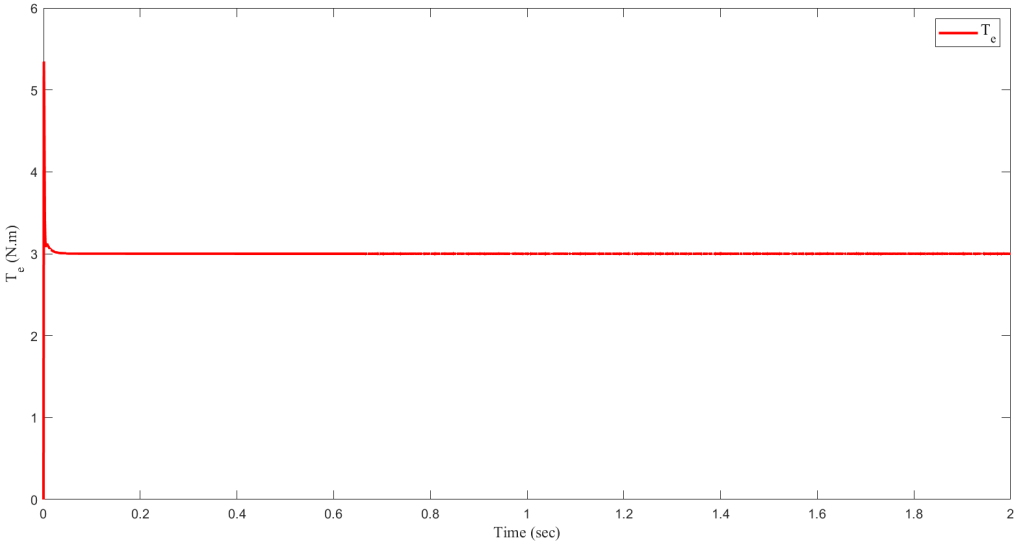

Figure 5.29: Electrical Torque of the Motor Under Load Torque

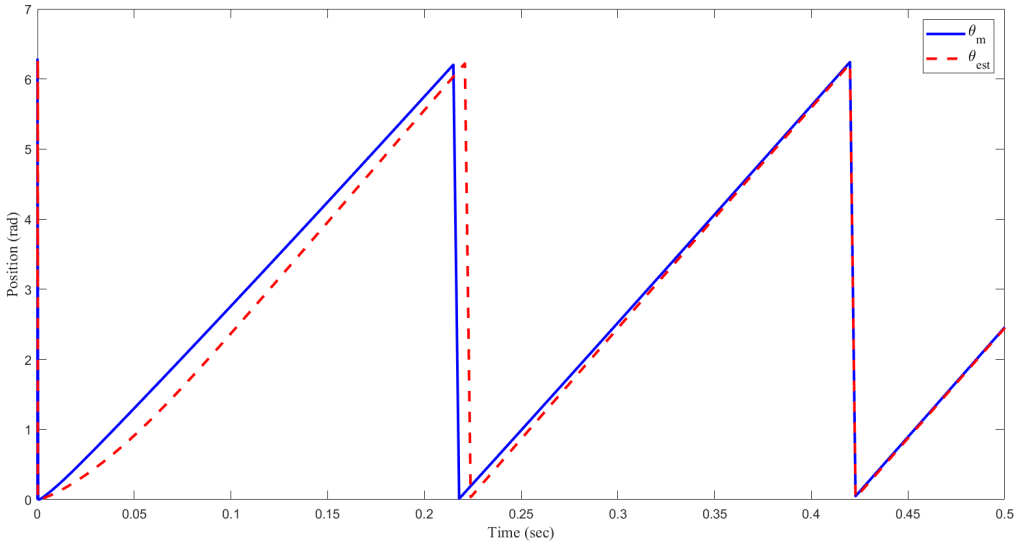

Figure 5.30: Position Measurement and Estimation Under Load Torque

5.7 Simulation Under Parameter Variation at 100 rad/sec

The fractional order sliding mode control and the adaptive super twisting sliding mode observer are both known for their robustness against parameter variation. To verify this,

a resistance value of the stator winding parameter was varied with adding a 10% on its nominal value and the following results are satisfactory.

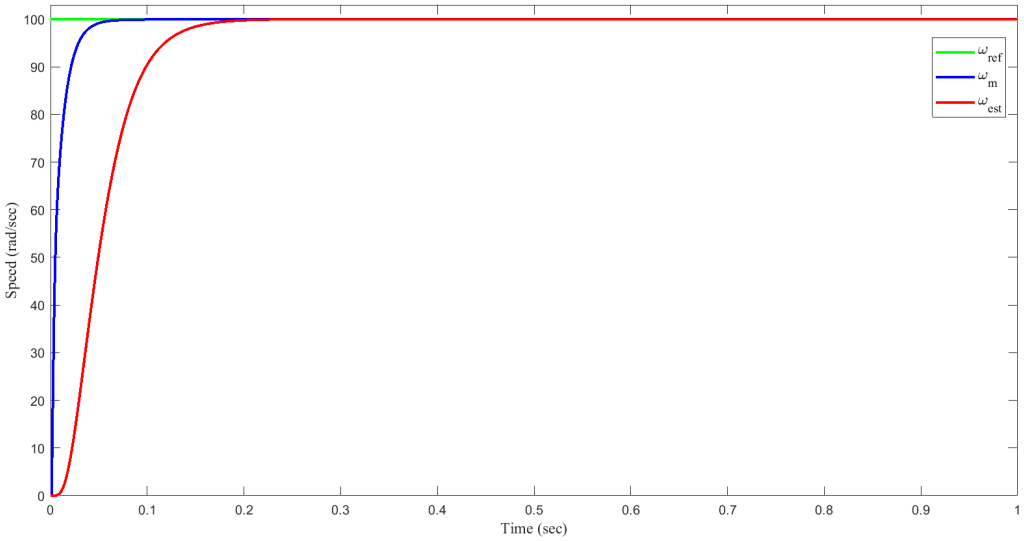

Figure 5.31: Speed Tracking Under Load Torque

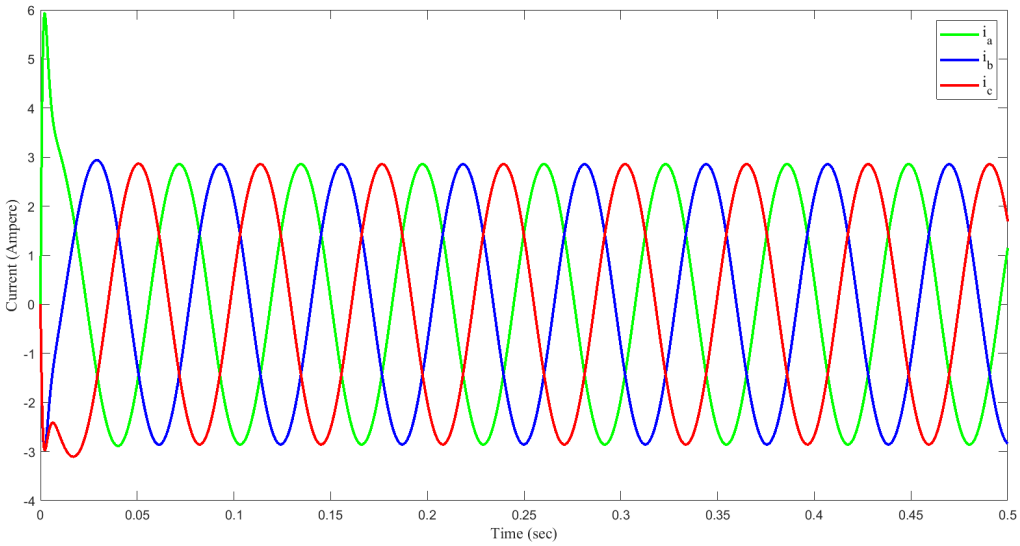

Figure 5.32: Three Phase Current Output of Motor Under Load Torque

5.8 Simulation Under Input Disturbance at 100 rad/sec

The speed control is mainly performed through the q-axis current. And usually input disturbance is introduced during the speed measurement and feedback for the speed control channel. From the previous simulation a maximum of 14 Ampere control signal was measured for speed control. Hence, 10% of this value is 1.4, so an input disturbance of this value was introduced and the following results verify the robustness of the FOSMC.

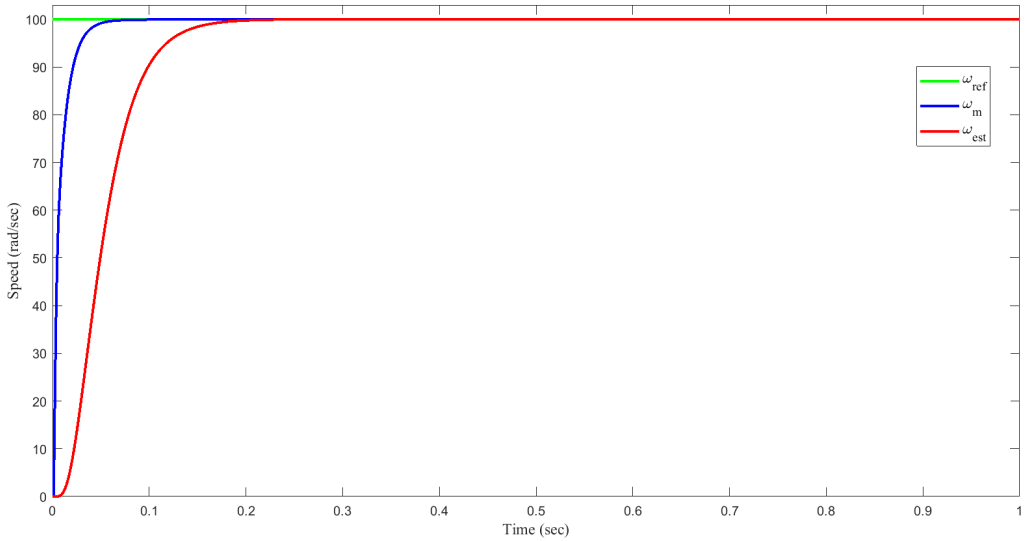

Figure 5.33: Speed Tracking Under Load Torque

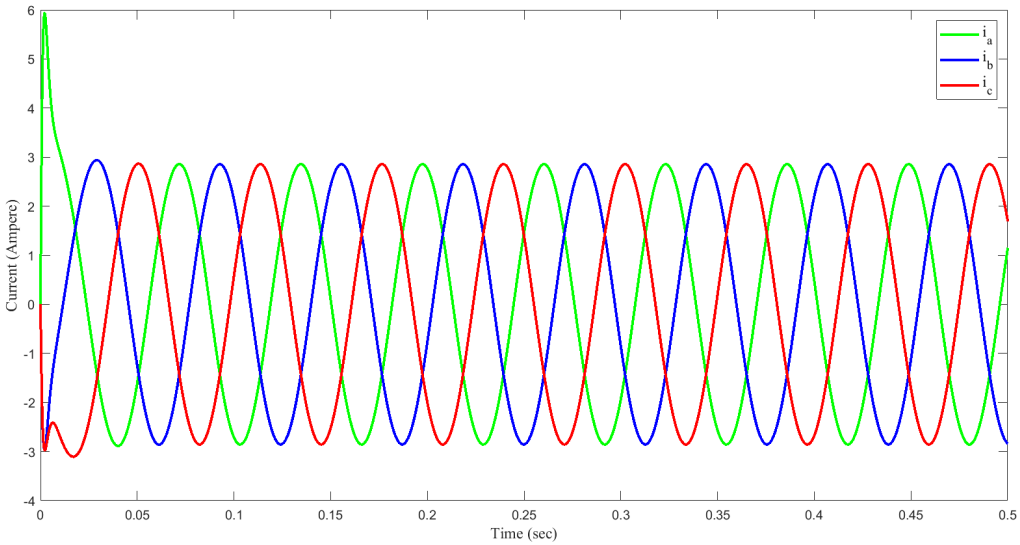

Figure 5.34: Three Phase Current Output of Motor Under Load Torque

5.9 Simulation Under Load Variation at 100 rad/sec

The nominal load of 3 Nm was changed to the value of 2 Nm at time t = 0.25 sec. The following figures show that the reduction in load respectively affects the required electrical torque, speed, currents and estimation of speed and position.

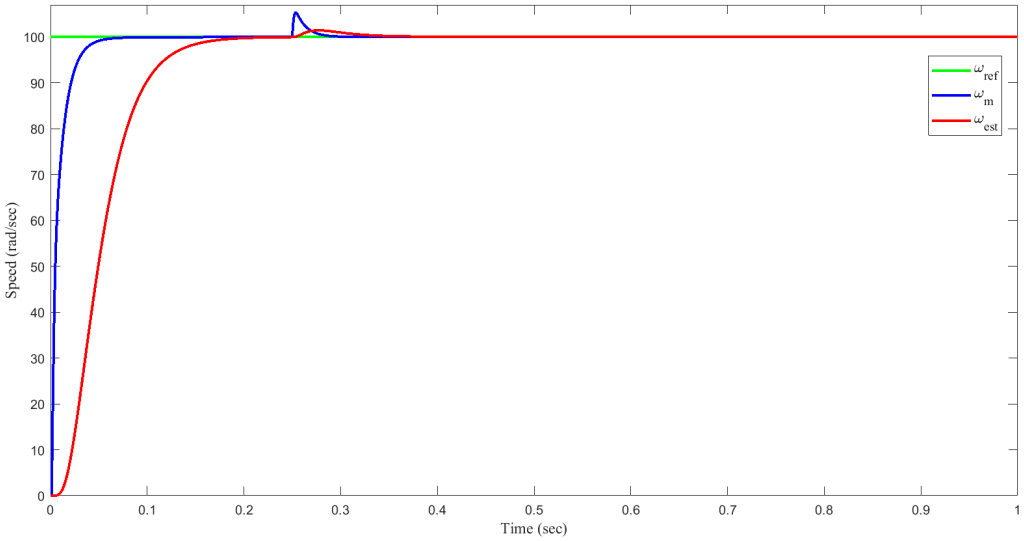

Figure 5.35: Speed Tracking Under Load Torque

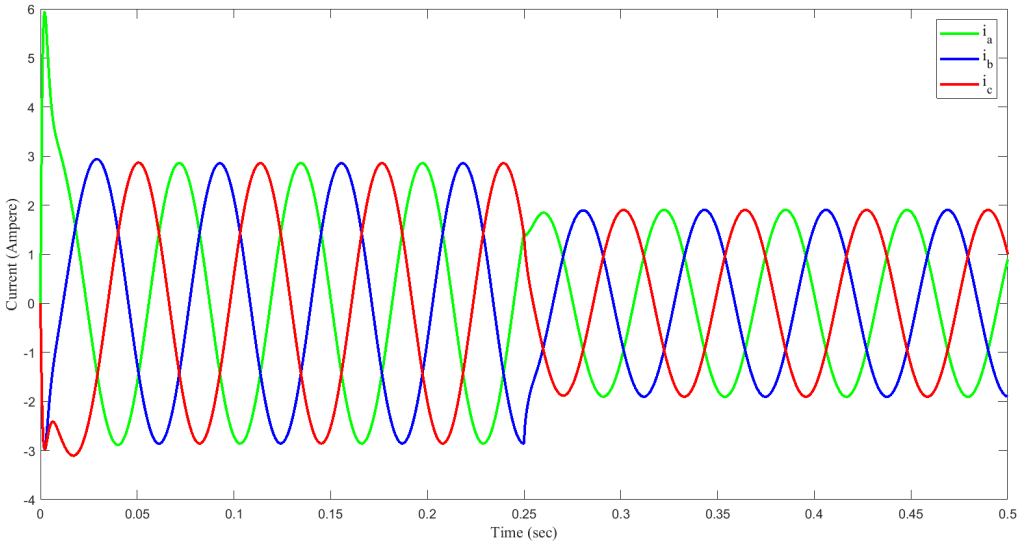

Figure 5.36: Three Phase Current Output of Motor Under Load Torque

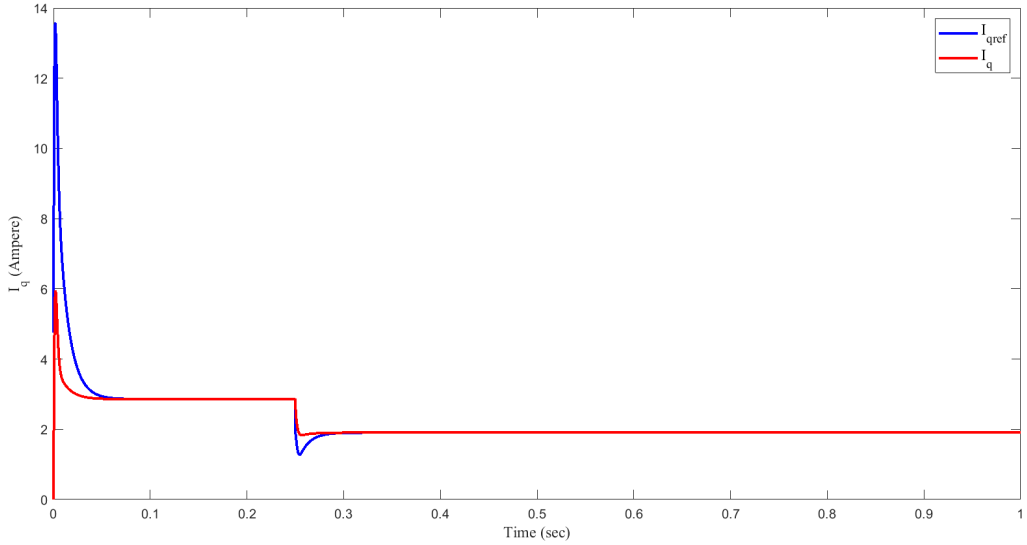

Figure 5.37: Current Tracking Along q-axis Under Load Torque

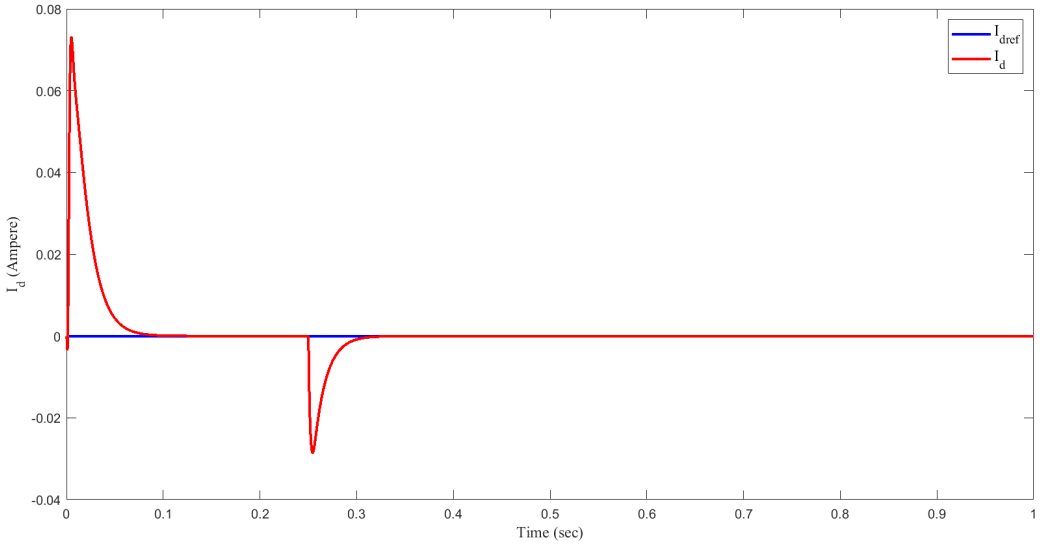

Figure 5.38: Current Tracking Along d-axis Under Load Torque

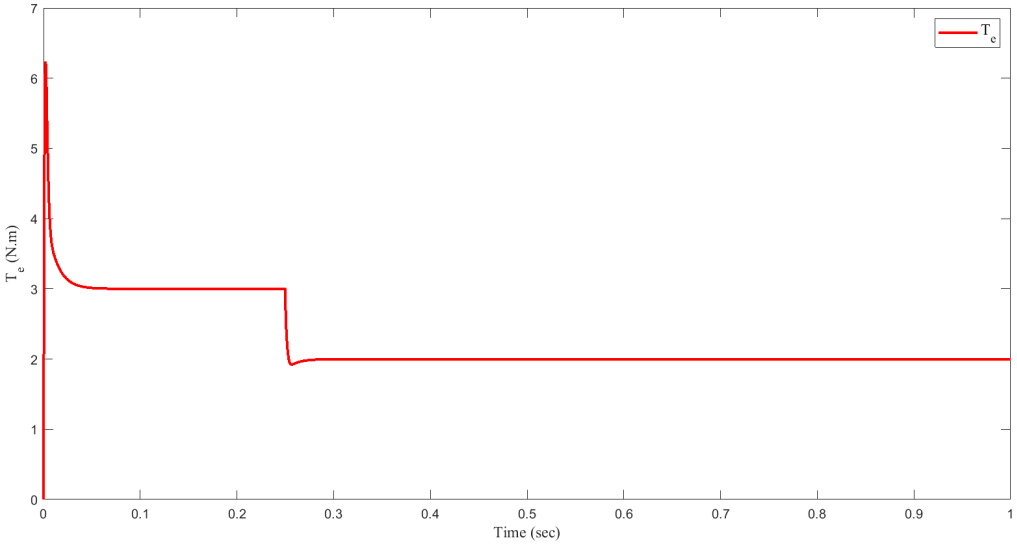

Figure 5.39: Electrical Torque of the Motor Under Load Torque

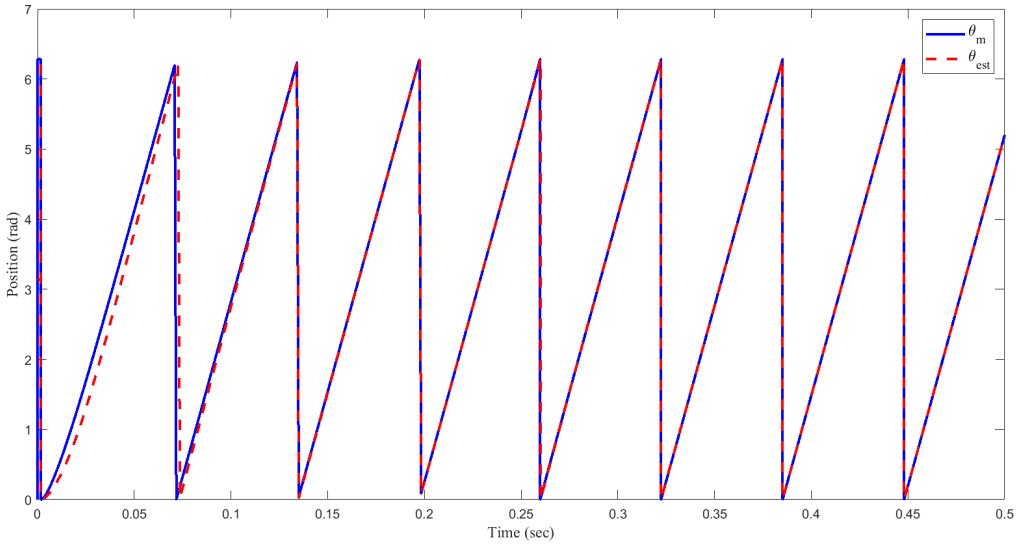

Figure 5.40: Position Measurement and Estimation Under Load Torque

5.10 Reversal Simulation Scenario

This section presents the setup and objectives of the reversal simulation scenario designed for a PMSM. The purpose of this simulation is to evaluate the motor's response to

a dynamic speed reversal command, examining the control system's ability to manage smooth transitions during acceleration to a positive rated speed and deceleration to a reversed negative speed.

The simulation sequence includes four distinct phases. In the initial phase, the motor accelerates linearly from rest to the rated speed of 300 rad/s over the first 2 seconds, testing the system's capability to reach the desired speed smoothly. This is followed by a constant positive speed phase, where the motor maintains a steady speed of 300 rad/s for a period of 3 seconds, from 2 to 5 seconds, simulating steady-state operation under typical positive rotational conditions. The third phase involves deceleration and reversal. Over a period of 3 seconds, from 5 to 8 seconds, the motor speed is gradually reduced from 300 rad/s to -300 rad/s, allowing for a controlled reversal that smoothly passes through zero speed. In the final phase, the motor operates at a constant negative speed of -300 rad/s, demonstrating steady-state performance under reversed conditions.

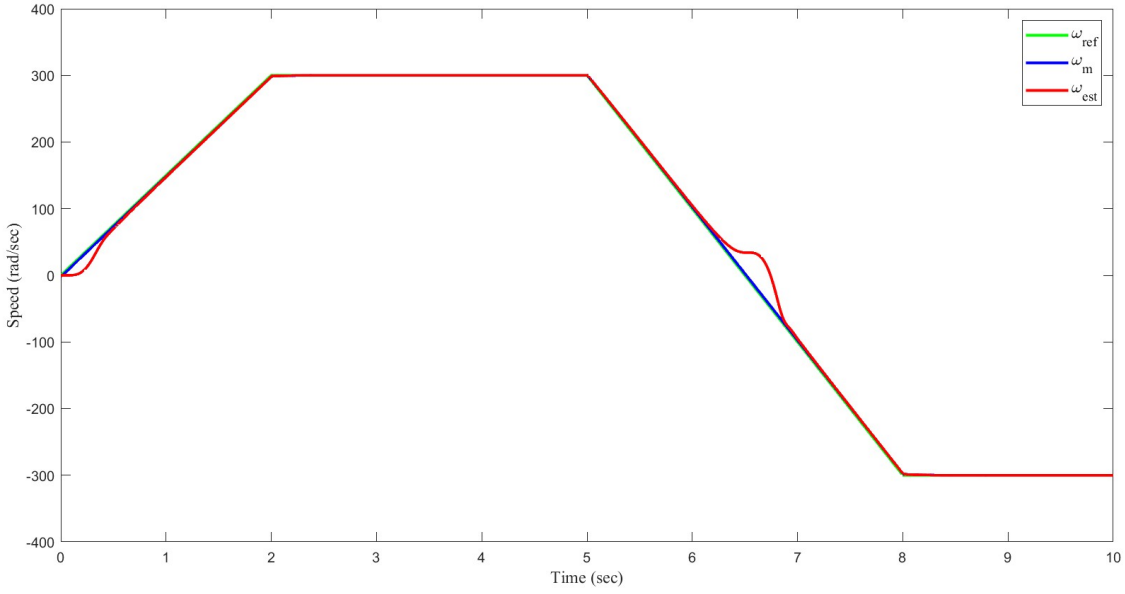

Figure 5.41: Speed Tracking Under Reversal Simulation

This reversal scenario provides critical insight into the performance of the FOSMC in both standard and reverse operational states. It highlights the controller's capacity to achieve stable transitions through zero speed and to maintain steady performance at

positive and negative rated speeds.

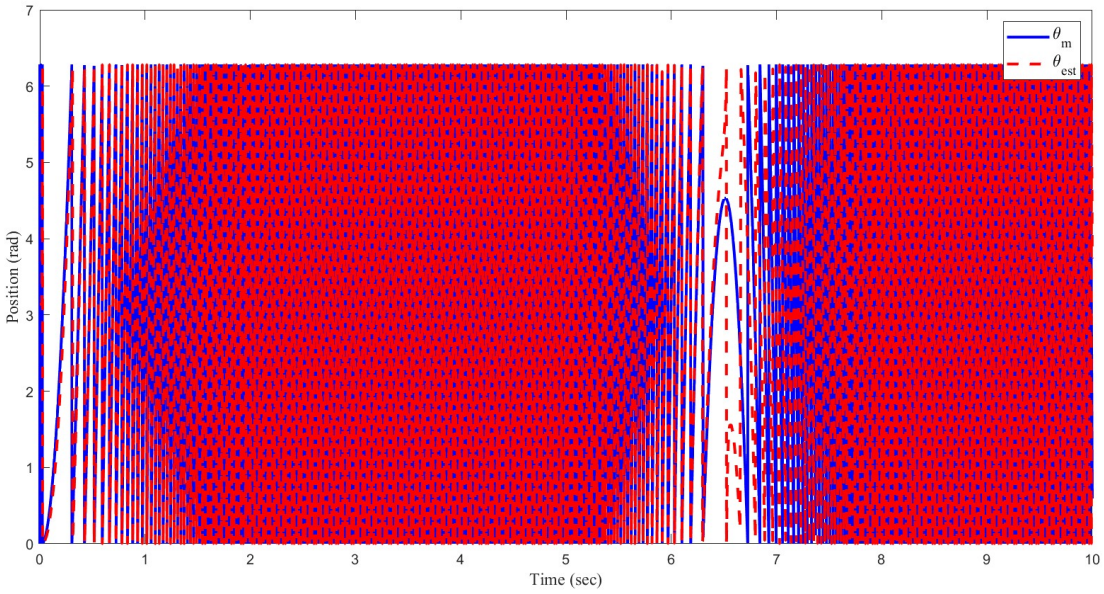

Figure 5.42: Position Measurement and Estimation Under Reversal Simulation

The plot presented in Figure 5.42 illustrates the position tracking performance of a PMSM control system during a reversal simulation scenario. The primary objective of this simulation is to assess the accuracy of the control system in tracking and estimating the motor's position amid dynamic speed changes, including phases of acceleration, constant speed, deceleration, and direction reversal. The degree of overlap between the measured and estimated position curves is indicative of the estimation accuracy of the designed controller. These curves alignment, demonstrates that the controller effectively maintains precise tracking throughout speed transitions and reversals. Any notable divergence between measured and estimated suggests potential inaccuracies in estimation, highlighting specific areas where enhancements needed in the controller or estimator, particularly in managing dynamic speed changes.

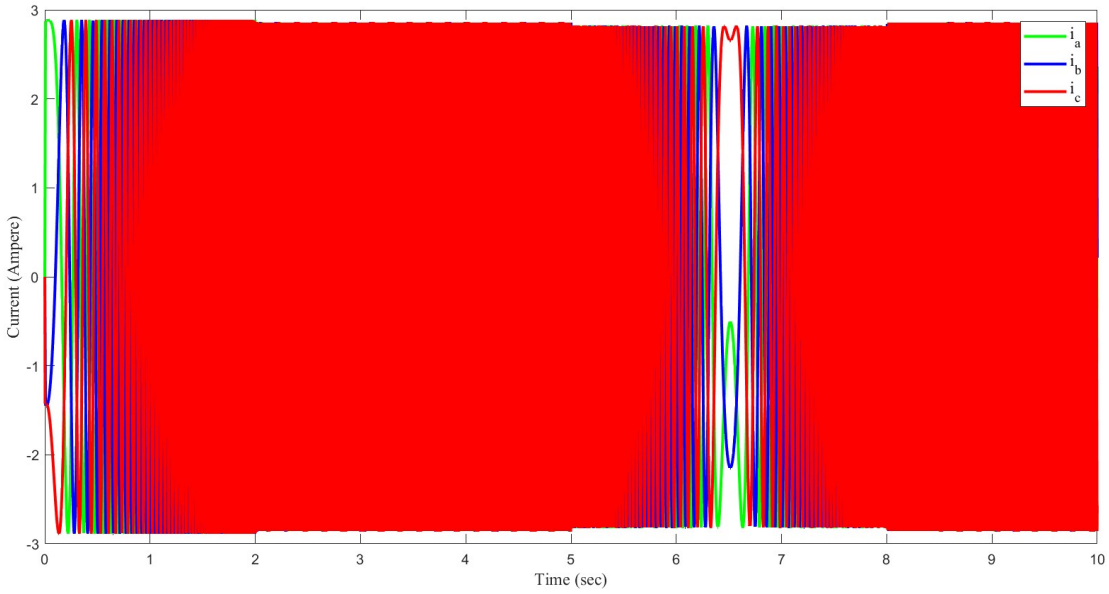

Figure 5.43: Three Phase Current Under Reversal Simulation

The results of this simulation are essential for applications requiring precise control and frequent direction changes, underscoring the reliability and robustness of the control system in dynamic environments.

Chapter 6

Conclusion and Recommendation

6.1 Conclusion

The simulation results of sensorless speed control for a PMSM utilizing FOSMC and STSMC speed and position estimator exhibit promising performance. Through the integration of FOSMC, the system achieves robust and accurate speed tracking in the absence of speed sensors. STSMC demonstrate excellent speed estimation capabilities, with mitigating chattering effects. These techniques effectively suppress disturbances and parameter uncertainties, ensuring stable motor operation across a range of operating conditions. Throughout the simulation, the FOSMC controller exhibited exceptional speed tracking performance, swiftly responding to changes in reference speed while maintaining stability and accuracy. This responsiveness was complemented by the robustness of the FOSMC approach, which proved effective in handling parameter variations and load disturbances.

Moreover, the SMC speed estimator demonstrated high accuracy in estimating the motor speed and position, even in the presence of measurement noise and uncertainties. This accurate estimation provided reliable feedback to the control system, contributing to its overall effectiveness. The transient response of the system was also noteworthy, with minimal overshoot and settling time observed during speed changes. This behavior indicates a well-tuned control system capable of swiftly responding to speed commands without introducing oscillations or instability.

In conclusion, the simulation results confirm the effectiveness of employing FOSMC with SMC speed estimation for controlling SPMSMs. The combined approach offers superior performance, robustness, and accuracy, making it suitable for various industrial applications requiring precise speed control of SPMSMs.

6.2 Recommendation

Comparative analysis with other control strategies may further underscore the advantages of FOSMC with SMC speed estimation in terms of performance, robustness, and complexity. Such comparisons can provide insights into the unique strengths of the proposed approach in SPMSM control applications.

The inner current control loops were done by a simple proportional-Integral (PI) control method. Hence, this can be further replaced with a more conventional and robust control like SMC. Further, validation through hardware implementation and real-world testing can reinforce the practical applicability of this control scheme.

References

[1] Y. Zhao, H. Yu, and S. Wang, "An improved super-twisting high-order sliding mode observer for sensorless control of permanent magnet synchronous motor," *Energies*, vol. 14, no. 19, p. 6047, 2021.

[2] F. Mohd Zaihidee, S. Mekhilef, and M. Mubin, "Robust speed control of pmsm using sliding mode control (smc)—a review," *Energies*, vol. 12, no. 9, p. 1669, 2019.

[3] P. Gao, G. Zhang, H. Ouyang, and L. Mei, "An adaptive super twisting nonlinear fractional order pid sliding mode control of permanent magnet synchronous motor speed regulation system based on extended state observer," *IEEE access*, vol. 8, pp. 53 498–53 510, 2020.

[4] J. R. Dominguez, A. Navarrete, M. A. Meza, A. G. Loukianov, and J. Canedo, "Digital sliding-mode sensorless control for surface-mounted pmsm," *IEEE Transactions on Industrial Informatics*, vol. 10, no. 1, pp. 137–151, 2013.

[5] S. Ziani, S. Essahel, Y. A. Zorgani, and M. Elghmary, "Control of permanent magnet synchronous motor by integrating the proportional-integral-derivative-regulation with backstepping," *ES Energy & Environment*, vol. 21, p. 842, 2023.

[6] T. Shi, Y. Yan, Z. Zhou, M. Xiao, and C. Xia, "Linear quadratic regulator control for pmsm drive systems using nonlinear disturbance observer," *IEEE Transactions on Power Electronics*, vol. 35, no. 5, pp. 5093–5101, 2019.

[7] M. A. M. Cheema, J. E. Fletcher, D. Xiao, and M. F. Rahman, "A linear quadratic regulator-based optimal direct thrust force control of linear permanent-magnet synchronous motor," *IEEE Transactions on Industrial Electronics*, vol. 63, no. 5, pp. 2722–2733, 2016.

[8] R. Molavi, K. Shojaee, and D. A. Khaburi, "Optimal vector control of permanent magnet synchronous motor," in *2008 IEEE 2nd international power and energy conference*. IEEE, 2008, pp. 249–253.

[9] L. M. Grzesiak and T. Tarczewski, "Permanent magnet synchronous motor discrete linear quadratic speed controller," in *2011 IEEE International Symposium on Industrial Electronics*. IEEE, 2011, pp. 667–672.

[10] G. G. Rigatos, M. Abbaszadeh, F. Marignetti, and P. Siano, "A nonlinear optimal control approach for voltage source inverter-fed three-phase pmsms," *COMPEL-The international journal for computation and mathematics in electrical and electronic engineering*, vol. 42, no. 6, pp. 1690–1717, 2023.

[11] J. Huang, H. Li, Y. Chen, Q. Xu *et al.*, "Robust position control of pmsm using fractional-order sliding mode controller," in *Abstract and Applied Analysis*, vol. 2012. Hindawi, 2012.

[12] A. G. Abo-Khalil, A. M. Eltamaly, M. S. Alsaud, K. Sayed, and A. S. Alghamdi, "Sensorless control for pmsm using model reference adaptive system," *International Transactions on Electrical Energy Systems*, vol. 31, no. 2, p. e12733, 2021.

[13] M. Shao, Y. Deng, H. Li, J. Liu, and Q. Fei, "Robust speed control for permanent magnet synchronous motors using a generalized predictive controller with a high-order terminal sliding-mode observer," *IEEE Access*, vol. 7, pp. 121 540–121 551, 2019.

[14] D. Eskezia, "Speed control of permanent magnet synchronous motor using higher order sliding mode controller."

[15] F. M. Zaihidee, S. Mekhilef, and M. Mubin, "Fractional order smc for speed control of pmsm," in *2018 International Electrical Engineering Congress (iEECON)*. IEEE, 2018, pp. 1–4.

[16] Q. Wang, S. Wang, and C. Chen, "Review of sensorless control techniques for pmsm drives," *IEEJ Transactions on electrical and electronic engineering*, vol. 14, no. 10, pp. 1543–1552, 2019.

[17] L. Prokop and P. Grasblum, "3-phase pm synchronous motor vector control using a 56f80x, 56f8100, or 56f8300 device," *Freescale Semi—conductor Application Note*, 2005.

[18] C. Gong, Y. Hu, J. Gao, Y. Wang, and L. Yan, "An improved delay-suppressed sliding-mode observer for sensorless vector-controlled pmsm," *IEEE Transactions on Industrial Electronics*, vol. 67, no. 7, pp. 5913–5923, 2019.

[19] H. Kim, J. Son, and J. Lee, "A high-speed sliding-mode observer for the sensorless speed control of a pmsm," *IEEE transactions on Industrial Electronics*, vol. 58, no. 9, pp. 4069–4077, 2010.

[20] V. C. Ilioudis, "Sensorless control of permanent magnet synchronous machine with magnetic saliency tracking based on voltage signal injection," *Machines*, vol. 8, no. 1, p. 14, 2020.

[21] T. Heikkilä *et al.*, "Permanent magnet synchronous motor for industrial inverter applications-analysis and design," 2002.

[22] V. M. Krishna, V. Sandeep, S. Murthy, and K. Yadlapati, "Experimental investigation on performance comparison of self excited induction generator and permanent magnet synchronous generator for small scale renewable energy applications," *Renewable Energy*, vol. 195, pp. 431–441, 2022.

[23] K. Sun, T. Summers, S. Janghorban, and H. Torresan, "Modelling multi-phase, low-speed permanent magnet machines for maritime propulsion applications," in *2019 29th Australasian Universities Power Engineering Conference (AUPEC)*. IEEE, 2019, pp. 1–8.

[24] A. Consoli, G. Scarcella, and A. Testa, "Industry application of zero-speed sensorless control techniques for pm synchronous motors," *IEEE Transactions on industry Applications*, vol. 37, no. 2, pp. 513–521, 2001.

[25] R.-M. Jan, C.-S. Tseng, and R.-J. Liu, "Robust pid control design for permanent magnet synchronous motor: A genetic approach," *Electric Power Systems Research*, vol. 78, no. 7, pp. 1161–1168, 2008.

[26] F. M. Zaihidee, S. Mekhilef, and M. Mubin, "Application of fractional order sliding mode control for speed control of permanent magnet synchronous motor," *Ieee Access*, vol. 7, pp. 101 765–101 774, 2019.

[27] P. Gao, G. Zhang, H. Ouyang, L. Mei *et al.*, "A sliding mode control with nonlinear fractional order pid sliding surface for the speed operation of surface-mounted pmsm drives based on an extended state observer," *Mathematical Problems in Engineering*, vol. 2019, 2019.

[28] S. Wu, J. Zhang, and B. Chai, "Adaptive super-twisting sliding mode observer based robust backstepping sensorless speed control for ipmsm," *ISA transactions*, vol. 92, pp. 155–165, 2019.

[29] Y.-S. Kung, V. Q. Nguyen, C.-C. Huang, and L.-C. Huang, "Simulink/modelsim co-simulation of sensorless pmsm speed controller," in *2011 IEEE Symposium on Industrial Electronics and Applications*. IEEE, 2011, pp. 24–29.

[30] J. A. Moreno and M. Osorio, "Strict lyapunov functions for the super-twisting algorithm," *IEEE transactions on automatic control*, vol. 57, no. 4, pp. 1035–1040, 2012.

[31] B. Derseh, L. Negash, and C. M. Abdissa, "Robust pso tuned fosmc for altitude stabilization and trajectory tracking of agricultural monitoring uav," *Authorea Preprints*, 2023.